

## PRACTICAL PHOTOEMISSION CHARACTERIZATION OF MOLECULAR FILMS AND RELATED INTERFACES

Ján Ivančo<sup>1</sup>

*Institute of Physics, Slovak Academy of Sciences, Dúbravská cesta 9, Bratislava, Slovakia*

Even though the term ‘organic electronics’ evokes rather organic devices, a significant part of its scope deals with physical properties of ‘active elements’ such as organic films and interfaces. Examination of the film growth and the evolution of the interface formation are particularly needful for the understanding a mechanism controlling their final properties. Performing such experiments in an ultra-high vacuum allows both to ‘stretch’ the time scale for pseudo real-time observations and to control properties of the probed systems on the atomic level. Photoemission technique probes directly electronic and chemical structure and it has thereby established among major tools employed in the field. This review primarily focuses to electronic properties of oligomeric molecular films and their interfaces examined by photoemission. Yet, it does not aspire after a complete overview on the topic; it rather aims to otherwise standard issues encountered at the photoemission characterization and analysis of the organic materials, though requiring to consider particularities of molecular films in terms of the growth, electronic properties, and their characterization and analysis. In particular, the fundamental electronic parameters of molecular films such as the work function, the ionization energy, and the interfacial energy level alignment, and their interplay, will be pursued with considering often neglected influence of the molecular orientation. Further, the implication on the band bending in molecular films based on photoemission characterization, and a model on the driving mechanism for the interfacial energy level alignment will be addressed.

PACS: 68.35.bm, 68.55.am, 71.20.Rv, 73.20.At, 73.22.-f, 79.60.Fr, 79.60.Dp

KEYWORDS: Photoemission, Molecular films, Organic semiconductors, Molecular orientation, Ionization energy, Work function, Energy level alignment, Band bending, Interfacial dipole, Organic-metal interface, Organic heterointerface, Organic-inorganic interface.

---

<sup>1</sup>E-mail address: Jan.Ivanco@savba.sk

## Contents

<b>List of symbols</b>	<b>209</b>
<b>List of acronyms/abbreviations</b>	<b>210</b>
<b>1 Introduction</b>	<b>211</b>
1.1 Energy levels in organic device . . . . .	211
1.2 Photoemission characterization of electronic structure of molecular films . . . . .	212
1.3 Oligomer molecular films . . . . .	215
1.4 Molecular orientation . . . . .	216
<b>2 Control of molecular orientation</b>	<b>219</b>
<b>3 Electronic properties</b>	<b>221</b>
3.1 Ionization energy, $E_I$ . . . . .	221
3.2 Work function, $\phi$ . . . . .	223
3.2.1 Molecular orientation-resolved intrinsic work function. . . . .	228
3.3 Molecular orientation-resolved growth modes . . . . .	229
3.4 The ionization energy-work function correlation . . . . .	232
3.5 Band bending deduction from photoemission . . . . .	233
3.6 $\pi$ band . . . . .	238
<b>4 Interfaces associated with molecular films</b>	<b>240</b>
4.1 Energy level alignment . . . . .	240
4.1.1 Equalization of electrochemical potentials . . . . .	243
4.2 On equivalency between the interfacial dipole and the vacuum-level offset . . . . .	247
4.3 Metal-on-organic interface . . . . .	248
<b>5 Summary</b>	<b>253</b>
<b>Acknowledgement</b>	<b>253</b>
<b>References</b>	<b>254</b>

## List of symbols

$e$	elementary charge, $1.602 \times 10^{-19}$ C
$E_B$	electron binding energy
$E_{EA}$	electron affinity
$E_F$	Fermi level
$E_G$	energy gap
$E_I$	ionization energy
$E_{I,el}$	(first) ionization energy of elements
$E_{I,film}$	(first) ionization energy of a film
$E_{I,org}$	(first) ionization energy of organics
$E_K$	electron kinetic energy
$E_{vac}$	vacuum level
$E_{vac,ML}$	vacuum level upon the formation of first monolayer
$E_{V_s}$	valence band edge on the surface,
$E_{seco}$	secondary electrons cut-off
$h$	Planck's constant, $6.626 \times 10^{-34}$ Js
$I_0$	(photoemission) intensity of a bare substrate
$I_{film}$	(photoemission) film-related intensity
$I_{subs}$	(photoemission) substrate-related intensity
$I_\infty$	(photoemission) intensity of a semiinfinite film
$m/e$	mass-to-charge ratio
$Q_D$	depletion zone charge
$Q_{ss}$	charge in surface states
$Q_{it}$	charge in interface states
$S$	slope parameter
$t$	film thickness
$U$	bias
$U_{an}$	voltage applied to the analyzer to detect an emitted electron
$U_{bi}$	build-in potential
$w$	depletion zone width
$\delta_i$	interface region thickness
$\Delta\phi_{L \rightarrow U}$	work function change induced by the orientational transition (of molecules)
$\Delta\phi_{ML}$	work function change upon growth of 1 <sup>st</sup> monolayer (ML)
$\Delta\phi_{ML(L)}$	work function change upon growth of 1 <sup>st</sup> ML formed by lying molecules
$\Delta\phi_{ML(U)}$	work function change upon growth of 1 <sup>st</sup> ML formed by upright-oriented molecules
$\Delta_{BB}$	band-bending magnitude
$\lambda$	electron inelastic mean free path
$\mu$	electrochemical potential
$\nu$	frequency
$\phi$	work function
$\phi_{an}$	work function of energy analyzer
$\phi_{film}$	work function of a film
$\phi_{ID}$	interface dipole potential
$\phi_{int}$	intrinsic work function
$\phi_{int,L}$	intrinsic work function of a film formed by lying molecules
$\phi_{int,U}$	intrinsic work function of a film formed by upright-oriented molecules
$\phi_s$	semiconductor work function
$\phi_{SD}$	surface-dipole potential
$\phi_{subs}$	work function of a substrate
$\varphi_e$	injection barrier for electrons
$\varphi_h$	injection barrier for holes

**List of acronyms/abbreviations**

*(Please, refer to Tab. 1.1 for the chemical formulae)*

BA	band alignment
BB	band bending
ELA	energy level alignment
HOMO	highest occupied molecular orbital
ID	interfacial dipole
FET	field-effect transistor
LNT	liquid nitrogen temperature
L→U	(orientational transition) from lying- towards upright-oriented molecules
LUMO	lowest unoccupied molecular orbital
ML	monolayer
OFET	organic field-effect transistor
OLED	organic light-emitting diode
OPC	organic photovoltaic cell
PCS	photoionization cross section
POD	preferentially-oriented diffusion
RT	room temperature
SAM	self-assembled monolayer
UHV	ultra-high vacuum
UPS	ultra-violet photoemission spectroscopy
VB	valence band
VL	vacuum level
VLA	vacuum-level alignment
wrt	with respect to
XPS	x-ray photoemission spectroscopy

## 1 Introduction

After some revived interest on conductivity of organic materials in early 1960's [1, 2] and on photovoltaic effect in 1975 [3], it was the breakthrough and pivotal work on transformation of transpolyacetylene into an electrical conductor with the conductivity controlled over several orders emerged in 1977 [4, 5], which installed a fresh oxymoron, namely 'organic electronics'. Nowadays, the term epitomizes both the class of devices based on organic electro- and opto-active materials, and such materials themselves. The latter are also denoted as conjugated materials or organic semiconductors owing to their resemblance to inorganic semiconductors in terms of the electronic and optical properties.

Since then, the research in the field has expanded considerably: the published works related to conjugated materials (the figure covers the research both on fundamental properties and organic devices, batteries, etc.) has inflated to as much as about several thousand studies to this day. In 2000, Heeger, Shirakawa, and MacDiarmid, who had triggered the new field, were awarded by Nobel Prize in chemistry '*For the discovery and development of conductive polymers*'.

Upon this, maiden demonstrations of devices based on the  $\pi$ -conjugated oligomer (*i.e.* small organic molecules with the fixed  $m/e$  ratio) films had followed, such as the single- [6, 7] and double-layer [8] organic photovoltaic cell (OPC), organic light-emitting diode (OLED) [9], and the organic field-effect transistor (OFET) [10, 11]. Recent trend has been oriented towards the replacement of oligomer by polymers with their pioneered employment in OLED [12], single-layer [13] and heterojunction-based [14] OPC, and OFET [15]. Particularly optical organic devices have been progressed far from their nascence and nowadays OLEDs and OPCs have reached a commercial rank.

Currently, the organic devices are second to traditional inorganic ones in terms of output parameters; nevertheless, the organic electronic materials offer various advantages. Besides the low-temperature (and thereby cheap) processing, the molecular design allows tuning of their fundamental electronic and optical properties, leading to a plethora of distinct materials with a tremendous potential for research and applications. In contrast to the class of inorganic semiconductors, where practically only several kind of semiconductors have been employable, hundreds new 'semiconducting' molecules produced and screened out up to date suggest the high figure of applicable materials. Along the molecular design determining fundamental electronic and optical properties of active molecular films, equally important are related interfaces, such as the interfaces between molecular films and contacting materials, or between distinct organic materials themselves. Therefore the interface engineering, hence the control of interfacial electronic properties, is the necessary prerequisite of the further progress in organic electronics. Even though the operating devices are routinely attained, the physics behind interfacial electronics is still not completely understood precluding an exploitation of the potential of organic electronics.

### 1.1 Energy levels in organic device

Figure 1.1 presents the energy diagram of a simple organic device under applied bias,  $U$ : an organic film is sandwiched between two metal electrodes with distinct work functions. Of relevance for transport properties are the injection barriers for electrons  $\varphi_e$  and holes  $\varphi_h$  tantamount to the energy level offset between the lowest unoccupied molecular orbital (LUMO) or highest occupied molecular orbital (HOMO), respectively, and the Fermi level of the contacting metal.

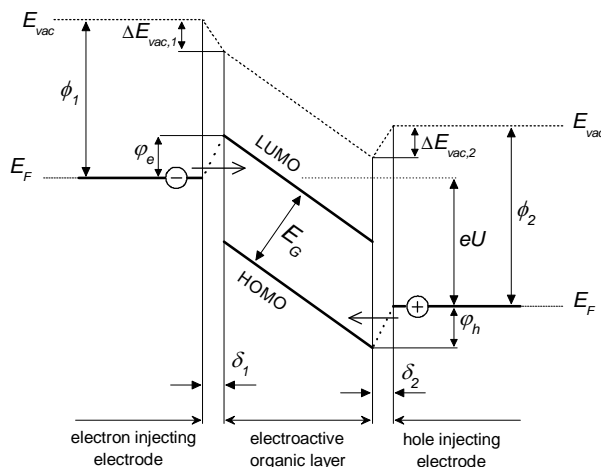


Fig. 1.1. A schematic energy diagram of an electroactive organic layer sandwiched between electrodes under bias,  $U$ . The  $\phi_i$  ( $i = 1, 2$ ) are the respective work functions of the metal electrodes 1 and 2, and  $\Delta E_{vac,i}$  ( $i = 1, 2$ ) are the vacuum level changes over the respective interface region thickness,  $\delta_i$ . The  $\phi_e$  and  $\phi_h$  are the injection barriers for electrons and holes. The  $E_G$  is the energy gap,  $E_F$  is the Fermi level.

The interfacial barrier for charge carriers can be indirectly evaluated from transport properties of final devices, or, alternatively, by photoemission. Particularly the latter approach is attractive, as the barrier can be determined directly by probing relevant energy levels, during the interface formation (the bottom-up manner) along the physical and chemical structure examined on atomic level.

## 1.2 Photoemission characterization of electronic structure of molecular films

Photoemission spectroscopy has been among the most traditional and potent techniques for the characterization of solid surfaces. Both chemical and electronic properties of solid surfaces and interfaces can be deduced. As for the mechanism, an electron from an occupied state is excited above the vacuum level by an impinging photon and can thus escape from the sample. The photoelectron kinetic energy of the ejected electron,  $E_K$ , allows to determine electron binding energy,  $E_B$ , via the Einstein relation:

$$E_B = h\nu - E_K \quad (1.1)$$

where  $h\nu$  is the photon energy of the incidence beam.

The standard laboratory photoemission facilities operate with x-ray sources thereby referred to x-ray photoemission spectroscopy (XPS). The most frequently used source based on the Al  $K\alpha$  excitation gives  $h\nu = 1486.6$  eV, the energy sufficient to probe at least some core levels of majority of elements. Aside the core-level spectroscopy commonly linked with the characterization of the chemical structure, the characterization of the valence band (VB) determining the electronic structure is of key importance for electronically active materials. Even though electronic structure can be studied by means of XPS too, the more convenient approach is the employment

of the ultra-violet photoemission spectroscopy (UPS). The typical light sources in UPS are rare gas discharges such as the He lamp with the photon energy of 21.22 eV. Compared to the  $\sim 1$  keV-photon source, the He lamp admittedly covers only a portion of the electron binding energy range, yet the photoemission cross section at low incident photon energy is several orders higher; for example, the shallow C  $2p$ , C  $2s$  orbitals, which are particularly relevant at examination of organic materials, have photoionization cross section higher by factor about  $10^5$  and  $2 \times 10^3$ , respectively, when excited by  $h\nu = 21.22$  eV compared to  $h\nu = 1486.6$  eV [16].

If a homogenous film over a substrate is grown, the substrate-related photoemission intensity,  $I_{subs}$ , is attenuated approximately according to the equation  $I_{subs} \propto I_0 \exp(-t/\lambda)$  for overlayer thickness exceeding one monolayer, where  $I_0$  is the intensity of the bare substrate,  $t$  is the overlayer thickness, and  $\lambda$  states for the electron inelastic mean free path. Thus, the overlayer thickness of  $\approx 3\lambda$  results in a drop of the substrate signal to about 5%. On the other side, the signal of a homogenous film,  $I_{film}$ , increases approximately according to formula  $I_{film} \propto I_\infty [1 - \exp(-t/\lambda)]$ , where  $I_\infty$  states for the signal of a semi-infinite film. Again, the formula works for the film thickness exceeding one monolayer. While the photon penetration depth is of the order of microns,  $\lambda$  is of the order of nanometres for XPS and as small as several angstroms for UPS making it extremely surface sensitive. This allows routine investigations of properties of adsorbents at deep-submonolayer coverages; since the substrate signal is fully eliminated by an overlayer with the thickness exceeding a few  $\lambda$ , comparable and smaller thicknesses of homogeneous overlayers can be determined with a high relative accuracy.

Regarding the interfaces, photoemission characterization permits the assessment of relative positions of energy levels, thereby the determination of interfacial electronic structure. Since the photoemission probing depth appears much smaller than the usually employed film thicknesses of the film/substrate systems, the interface properties are conveniently investigated by means of so-called surface-science approach [17, 18]: the film is grown in a stepwise manner under ultra-high vacuum (UHV) conditions at pressures  $< 10^{-9}$  mbar onto atomically clean and controlled substrates, while the evolutions of electronic, chemical, structural, and morphological properties are simultaneously examined *in situ* at the onset of the interface formation. This allows the determination of factors governing the interface properties such as  $\varphi_h$  (Fig. 1.1). The surface-science approach benefits from the well-described and defined film/substrate systems under studies at atomic level free from ambient influence.

Figure 1.2 illustrates the valence band (VB) of a molecular film, here of copper phthalocyanine (CuPc), grown on a substrate. The VB of a molecular film comprises of a number of shallow nearby molecular orbitals. Their relative positions are weakly affected by the intermolecular interaction occurring in condensed films [19]. Since the shallowest orbitals are shaped by  $\pi$  bonds of a molecule, the VB region near the Fermi level is referred to as the  $\pi$  band. Of orbitals constituting the VB, the HOMO is considered as the cardinal one; in terms of the molecular film, the energy difference between the HOMO and LUMO is termed the HOMO-LUMO gap, which determines the optical and transport band gap. As for a contact between a molecular film and a metal, the HOMO referred to the Fermi level is termed the band alignment (BA), or energy level alignment (ELA), and it corresponds to the transport barrier for holes  $\varphi_h$  injected from a metallic substrate to organics (Fig. 1.1). We note that  $\varphi_h$  is ascertainable by the (direct) photoemission,  $\varphi_e$  can be probed by an inverse photoemission. The HOMO referred to the vacuum level,  $E_{vac}$ ,

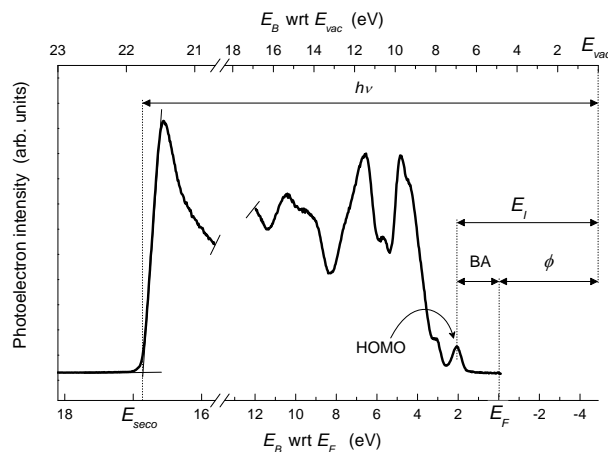


Fig. 1.2. The valence band of copper phthalocyanine (CuPc) film with indication of fundamental electronic parameters such as the band alignment (BA), ionization energy ( $E_I$ ), and work function ( $\phi$ ); the latter makes the difference between the energy scales referred with respect to (wrt) the Fermi level (bottom) and the vacuum level (upper),  $h\nu$  corresponds to photon energy of the incident beam,  $E_{seco}$  is the secondary electrons cut-off.

identifies with the ionization energy,  $E_I$ . Obviously,

$$E_I = BA + \phi, \quad (1.2)$$

where  $\phi$  states for the electron work function. The essential problem of the interface engineering would be the understanding a mechanism controlling the BA. That has motivated numerous photoemission studies focused on the examination of HOMO binding energies for various molecular films grown on a variety of substrates to reveal a correlation between electronic properties of isolated materials, hence prior to the contact formation, and the band alignment.

The edge at the high- $E_B$  side of the valence band in Fig. 1.2 manifests the onset of the secondary electrons cut-off ( $E_{seco}$ ). Its position determines  $\phi$ , which is defined as the minimal energy necessary to transfer an electron from the material to the nearby vacuum with its final kinetic energy being zero. The work function is obtained as  $\phi = h\nu - E_{seco}$ .

Note that the HOMO position is assigned to its maximum energy in Fig. 1.2. This is in variance with a frequent approach identifying the HOMO position with the low- $E_B$  onset of the HOMO approximated by its leading edge. The use of the onset had been substantiated in relation with optical properties, since the energy gap determined by optical absorption better suits the position of the HOMO and the LUMO onsets (see *e.g.* Refs. [20] and [21]). Yet, the peak shape is affected by experimental factors such as instrumental resolution or sample temperature. Moreover—unlike *e.g.* the onsets of the secondary electrons and the Fermi edge—the HOMO peak shows no leading edge, accordingly no linear portion. Particularly at low intensities, the ‘leading edge’ of the HOMO can result in an uncertain determination of its binding energy. We therefore advocate the former approach eventually amended by a correction. Nevertheless, the experimentally determined HOMO values addressed in this study were prevalingly



dug out in the literature—where the low- $E_B$  onset had been commonly preferred for the HOMO determination—and thereby adopted for our purposes as they were.

### 1.3 Oligomer molecular films

Even though the polymers dominate in the role of active layers particularly in nowadays commercial organic devices, a great deal of knowledge on organic films was achieved by means of studies on model oligomer molecules. In contrast to the polymers, the oligomers can be sublimed in UHV making them employable for the surface-science approach. That—although not intended to be technologically competitive for the production of organic devices—oriented towards small molecules permits studies on fundamental chemical and electronic issues. Table 1.1

Tab. 1.1. Overview of molecular films tackled in this work.

Acronym	Chemical formula	Name
6P	C <sub>36</sub> H <sub>22</sub>	sexiphenyl
6T	C <sub>24</sub> H <sub>14</sub> S <sub>6</sub>	sexithiophene
$\alpha$ -NPD, NPB	C <sub>44</sub> H <sub>32</sub> N <sub>2</sub>	<i>N, N'</i> -diphenyl- <i>N, N'</i> -bis(1-naphthyl)-1,1'-biphenyl-4,4'-diamine
Alq <sub>3</sub>	C <sub>27</sub> H <sub>18</sub> AlN <sub>3</sub> O <sub>3</sub>	tris(8-hydroxyquinoline)aluminum
BCP	C <sub>26</sub> H <sub>20</sub> N <sub>2</sub>	bathocuproine
BP2T	C <sub>32</sub> H <sub>22</sub> S <sub>2</sub>	2,5-bis(4-biphenyl) bithiophene
CBP	C <sub>36</sub> H <sub>24</sub> N <sub>2</sub>	4,4'- <i>N, N'</i> -dicarbazolyl-biphenyl
CuPc	C <sub>32</sub> H <sub>16</sub> CuN <sub>8</sub>	copper phthalocyanine
DH4T	C <sub>20</sub> H <sub>26</sub> S <sub>4</sub>	$\alpha\omega$ -dihexyl-quaterthiophene
DH6T	C <sub>36</sub> H <sub>38</sub> S <sub>6</sub>	$\alpha\omega$ -dihexyl-sexithiophene
DiMe-PTCDI	C <sub>26</sub> H <sub>14</sub> O <sub>4</sub> N <sub>2</sub>	<i>N, N'</i> -dimethyl-3,4,9,10-perylenetetracarboxylic diimide
F <sub>4</sub> CuPc	C <sub>32</sub> H <sub>12</sub> F <sub>4</sub> CuN <sub>8</sub>	tetrafluoro copper phthalocyanine
F <sub>4</sub> TCNQ	C <sub>12</sub> F <sub>4</sub> N <sub>4</sub>	2,3,5,6-tetrafluoro-7,7,8,8-tetracyanoquinodimethane
F <sub>16</sub> CuPc	C <sub>32</sub> F <sub>16</sub> CuN	hexadecafluoro copper phthalocyanine
H <sub>2</sub> Pc	C <sub>32</sub> H <sub>18</sub> N <sub>8</sub>	metal-free phthalocyanine
HBC	C <sub>42</sub> H <sub>18</sub>	hexa- <i>peri</i> -hexabenzocoronene
HATCN	C <sub>18</sub> N <sub>12</sub>	hexaazatriphenylene-hexacarbonitrile
NADPO	C <sub>20</sub> H <sub>32</sub> O <sub>4</sub> N <sub>4</sub>	amphiphilic substituted 2,5-diphenyl-1,3,4-oxadiazole
NiPc	C <sub>32</sub> H <sub>16</sub> NiN <sub>8</sub>	nickel phthalocyanine
NTCDA	C <sub>14</sub> H <sub>4</sub> O <sub>6</sub>	1,4,5,8-naphthalene tetracarboxylic dianhydride
PEN	C <sub>22</sub> H <sub>14</sub>	pentacene
PFP	C <sub>22</sub> F <sub>14</sub>	perfluoro-pentacene
PTCBI	C <sub>36</sub> H <sub>16</sub> O <sub>2</sub> N <sub>4</sub>	3,4,9,10-perylenetetracarboxylic bisbenzimidazole
PTCDA	C <sub>24</sub> H <sub>8</sub> O <sub>6</sub>	3,4,9,10-perylenetetracarboxylic dianhydride
PTCDI	C <sub>24</sub> H <sub>10</sub> O <sub>4</sub> N <sub>2</sub>	3,4,9,10-perylenetetracarboxylic diimide
TCNQ	C <sub>12</sub> H <sub>4</sub> N <sub>4</sub>	tetracyanoquinodimethane
ZnPc	C <sub>32</sub> H <sub>16</sub> ZnN <sub>8</sub>	zinc phthalocyanine
ZnTPP	C <sub>44</sub> H <sub>28</sub> N <sub>4</sub> Zn	5, 10, 15, 20-zinctetraphenylporphyrin

lists the oligomers addressed in this study. Their chemical structures are collected in Fig. 1.3.

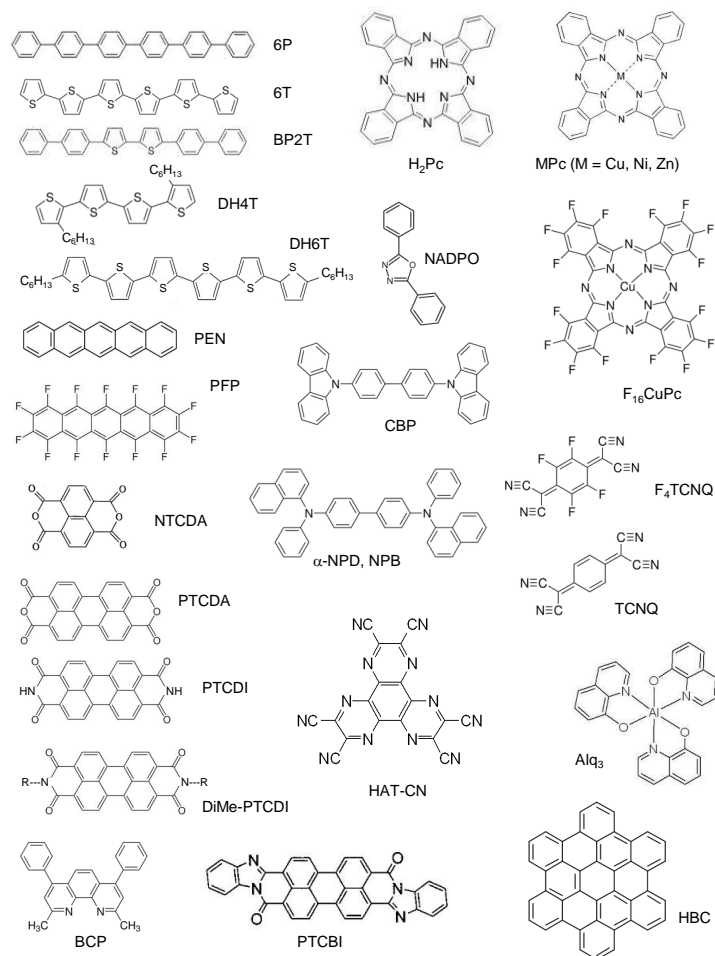


Fig. 1.3. The structural formulae of oligomer molecules listed in Tab.1.1.

#### 1.4 Molecular orientation

Figure 1.4a shows the  $\pi$  orbitals of benzene ring oriented along the normal of the ring plane. The overlapped orbitals form a conjugated system with the delocalized electrons. Molecular crystals are noted for anisotropic electronic properties: for example, transport properties of an organic device are dramatically affected by the molecular orientation relative to the current flow [22]. The most efficient current flow in a molecular film occurs along the direction of the stacked  $\pi$

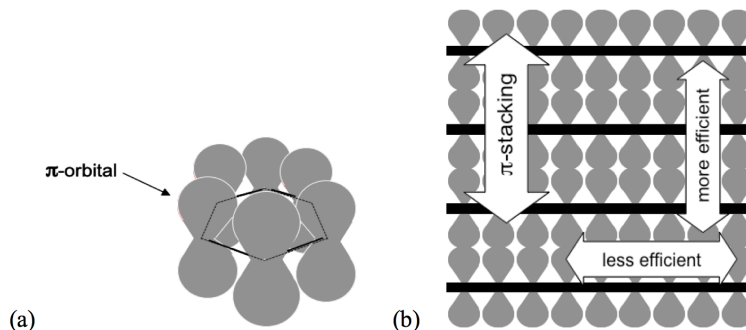


Fig. 1.4. The schematic views on (a) the spatial distribution of  $\pi$  orbitals of a benzene ring represented by a hexagon, and (b) the assembly of ordered molecules viewed along their ring planes with indicated  $\pi$ -stacking direction. The thick lines represent backbones of the molecules. The directions with the more and less efficient charge carrier transport are shown.

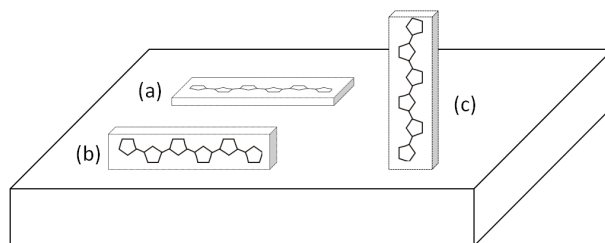


Fig. 1.5. Characteristic orientations of a molecule (here, exemplified by sexithiophene) with respect to the substrate surface: the lying molecule oriented flat-on (a) and edge-on (b), and the upright-oriented (end-on) molecule (c).

bonds being coincident with the interaction between the  $\pi$  bonds of neighbouring molecules. This is illustrated in Fig. 1.4b schematically presenting the side view of an ordered assembly of molecules, *e.g.* of pentacene.

Herringbone structure of crystalline molecular films implicates the different orientations of particular molecules within the unit cell, yet, an average molecular orientation pertinent to a film can be addressed; thus, the term ‘molecular orientation’ describes the average orientation of molecules in a molecular film in terms of the orientation of the molecular plane and/or its backbone with respect to the surface normal. The molecules with their backbones parallel or near parallel to the substrate *surface* are referred to the lying ones (Fig. 1.5a,b). The molecules with their molecular planes and/or backbones parallel or near parallel with the surface *normal* have upright orientation (Fig. 1.5c). Obviously, the term molecular orientation refers to the orientation of molecules embedded in the crystalline film.

Depending on the targeted planar device—typical contrasting examples being the OLED and the OFET—the current flows in the device parallel either to the substrate surface normal



Fig. 1.6. Examples on organic devices with distinct targeted molecular orientation (the molecules are emblemized by ovals): the lying orientation for the OLED (left) and the upright orientation for the OFET (right). Molecular layer are sandwiched between contacting layers. The arrows indicate the current flow directions.

or to the substrate surface (Fig. 1.6). Likewise, the molecular orientation determines interfacial energetics and by controlling the relative molecular orientation at the donor/acceptor interfaces in organic heterostructures the charge transfer [23] and charge dissociation [24] can be affected. It is therefore essential to control both the crystallinity of grown films and the molecular orientation.

## 2 Control of molecular orientation

To control the molecular orientation, the mechanism of the organic film growth has been widely studied via the molecule deposition on a variety of substrates; typical examples include reconstructed surfaces of single-crystal metallic substrates, inorganic semiconductors, and oxidized surfaces. The profound influence of the substrate nature on the film structure and packing were frequently demonstrated. Yet, this mostly concerned of thin films, as further growth towards thick films resulted in the different film structure and morphology weakly or not dependent on the substrate.

Commonly, the rod-like molecules, such as *e.g.* 6P, 6T, pentacene, adsorb onto metallic substrates with the lying geometry. According to the conventional wisdom, the principal factor determining the lying molecular orientation had been assumed to be the high interaction strength between molecular  $\pi$  bonds and the surface of metallic substrate, while the upright-oriented molecules in films grown on oxidized surfaces such as  $\text{SiO}_2$ ,  $\text{Al}_2\text{O}_3$ , glass, etc., were rationalized by the weak(er) interaction of molecules to the surfaces passivated by oxygen [25-32].

Exceptions from the interaction-strength model, such as the upright molecular orientation in films grown onto polycrystalline and non-oxidized metallic surfaces (Au, Ag, and Cu) were substantiated by the higher roughness of the polycrystalline surfaces compared to the single-crystal surfaces [33-35]. Though, the interaction-strength model implicates further inconsistencies. For example, it does not rationalize the lying orientation of molecules beyond the first monolayer of the molecular film; whereas the first monolayer acts as a substrate for the second monolayer, the weak molecule-molecule interaction should result to universal upright orientation by the second layer upon the closing the first layer. Such scenario—although reported occasionally—is in contrast with frequent observations.

According to Ref. [36], the molecular orientation is controlled by the substrate surface topology such as the presence of the long-range surface order or by lack of it, instead of the interaction strength between the molecule and the substrate. Specifically, a diffusion of molecules over the substrate surface either along preferred directions or in azimuthally random directions was proposed to be the principal factor determining the molecular orientation [37]; the adsorbed molecules, which do not chemically react with the substrate, diffuse over the substrate surface till they are embedded into the formed organic crystal. The necessary requirement for getting the lying orientation in the film is the presence of a diffusion director on the substrate surface. Preferential azimuthal directions present on reconstructed surfaces manifested by a lower energy for the molecular diffusion [38], or unoriented steps on vicinal surfaces [39], or directed scratches [40], can act as directors. The molecules diffusing over preferred azimuthal direction result in the growth governed by attractive intermolecular interaction for the probability for a molecule of being involved in a crystal growth seemingly increases if diffusing molecules encounter aligned; this maximizes the overlap of  $\pi$  bonds between the neighbouring molecules and thereby preserves the lying orientation upon their embedding in the film [36, 41]. The deficient or intentionally marred surface reconstruction (*e.g.* by sputtering) has a dramatic effect on the film growth; instead of the lying molecular orientation, the molecules orient upright, thus sharply disproving the interaction strength model [36, 42]. This is due to the diffusion of the molecules over an unordered surface, thus in random directions, which results in the formation of energetically more favourable crystals made of upright-oriented molecules. Obviously, a single molecule adsorbs with the lying geometry and preserves it while diffusing over both ordered and disordered



Fig. 2.1. Sketched illustration of the gradual L→U orientational transition (from lying- towards upright-oriented molecules): the molecular tilt angle gradually varies with the increased thickness of a molecular film (from left to right). The  $\phi_L$  and  $\phi_U$  state for the work function corresponding the molecular film surface formed by lying- and upright-oriented molecules, respectively.

surface; the lying and upright molecular orientations are meant in terms of the final orientation of embedded molecules.

It should be noted that the lying geometry, if achieved on proper substrates, usually applies for thin and up to moderately thick films only, and the molecular orientation changes towards the upright with the further film growth (Fig. 2.1). In other words, such molecular films are inhomogeneous in terms of the molecular orientation. The orientational change with the increasing film thickness from lying to upright is termed the L→U orientational transition. The orientational transition can occur either abruptly already by the second layer [43-45], or gradually within the nominal film thickness ranging from several nanometres up to several tenths of nanometre [27, 39, 46-49]. The upright molecular orientation was reported also to be owing to the higher growth temperature [43, 50]. The gradual orientational transition with the film thickness was reported for polymers too [51] and it may be a general growth phenomenon, although it has been often unnoticed. Importantly, the orientational transition affects the film electronic properties. Indeed, in terms of electronic properties, the molecular film with the orientational transition is a heterostructure. This will be discussed in the next chapters.

In general, the upright orientation is easier to achieve and it particularly takes place (i) at elevated growth temperatures, owing to the high kinetic energy sufficient to free the diffused molecules confined by the director, (ii) on unordered or poorly ordered surfaces lacking the directors.

By elevating the substrate surface morphology to the primary factor determining the molecular orientation in the film, the preferentially-oriented diffusion (POD) model justifies distinct molecular orientations obtained on chemically identical but topologically distinct surfaces, such as the reconstructed and polycrystalline metallic surfaces [34-35]; the lack of the POD on the latter results in upright oriented molecules in the film, while the lying molecular orientation takes place on the reconstructed/ordered surface. The chemical origin of the substrate plays a minor role unless the adsorbed molecule is immobilized by chemical reaction with the substrate.

The POD model rationalizes the frequently observed and undesirable gradual orientational transition occurring in thicker film (Fig. 2.1); the surface order of molecular films deteriorates with the increasing film thickness due to growth imperfectness and thereby the directors [ $n$ th layer on the film acts as the substrate for the ( $n + 1$ )th layer] gradually deteriorate and vanish. This results in the gradual orientational transition affecting the electronic properties (see the discussion on growth fashions and the band bending below). On the other hand, distinct molecular orientation affects the crystal orientation with respect to the substrate, yet the crystal structure can remain preserved as it was suggested by the vibronic progressions insensitive to the molecular orientation [52].

### 3 Electronic properties

#### 3.1 Ionization energy, $E_I$

Equivalent to the first ionization energy of elements, the ionization energy of a molecule is the minimal energy necessary for the removal of an electron from the HOMO and move it to infinity. The binding energies of an isolated molecule (in the gas phase) have to be referred to the vacuum level and the first ionization energy is a material constant. In photoemission characterization of solid surfaces, the Fermi level reference has been the convenient reference choice, since the Fermi level of grounded sample coincides with the ground of spectrometer. Thereby, the energy scale is shifted by the surface work function,  $\phi$ , from the absolute energy scale referred to the vacuum level (recall both energy scales in Fig. 1.2).

The ionization energy of a condensed molecule constituting the molecular film is lower typically by about 1 eV in comparison to the ionization energy of that but isolated molecule due to the extra-molecular screening present in condensed phase [53]. Molecules embedded in the bulk of the molecular film and those terminating its surface experience distinct surroundings which is reflected in their photoemission spectra [54].

The ionization energies of the oligomer molecular films listed in Tab. 1.1 range from about 4.4 eV to almost 10 eV reported for 6T [27] and HAT-CN [55], respectively. In a first approximation, the constituting elements with the high ionization energy, such as N, O, and/or F, tend to increase the ionization energy of the molecule compared to the hydrocarbon molecule comprised exclusively of C and H; for example, the substitution of hydrogen in the C-H bonds by fluorine leads to substantial increase of the ionization energy, as seen for and fluorine-substituted TCNQ [56], phthalocyanines [20, 57], PEN [58], and alkanethiols with different end groups [59].

Unlike an isolated molecule, which has a unique ionization energy, the ionization energy of a condensed molecular *film* may show distinct values; the difference of 0.35 eV has been initially reported for differently prepared sexiphenyl films [60]. This is illustrated in Fig. 3.1, where the upper  $\pi$  band of the 6P films grown at RT and 395 K are contrasted. For the spectra are referenced to the vacuum level, the HOMO offset indicates difference in the ionization energies. The varying ionization energy suggests that it is not a material constant and the growth conditions such as *e.g.* the substrate surface properties and temperature can lead to changes in  $\pi$ -band electronic structures. Importantly, this may extend the possibility to control the band alignment and thereby the transport barrier at the contact.

The observed  $\Delta E_I$  was assumed to be the result of initial and/or final state differences. The former can occur due to differences in  $\pi$  conjugation as a result of varying interring (torsional) angle between neighbouring benzene rings induced by the spherical hinderance of hydrogen atom. The latter can arise from differences in the screening of the photo-hole. Both differences can be affected by the packing in the molecular solid and are to a certain extent interrelated.

Figure 3.2 shows the evolution of  $E_I$  with the 6T film thickness for films grown at liquid nitrogen temperature (LNT) and RT on  $\text{SiO}_x$  substrates. For the LNT growth,  $E_I \approx 5.8$  eV results whether measured at LNT or after warming to RT. This value matches reasonably well the value of 5.9 eV derived from  $E_I$  of the gas phase being of 7.0 eV [61] and corrected for extra-molecular screening of 1.1 eV, which is common in organic solids [53] and suggests a 'frozen' gas phase. The ionization energy of the LNT-grown film is nearly independent on the film thickness, while that of the RT-grown film dramatically drops with the film thickness by

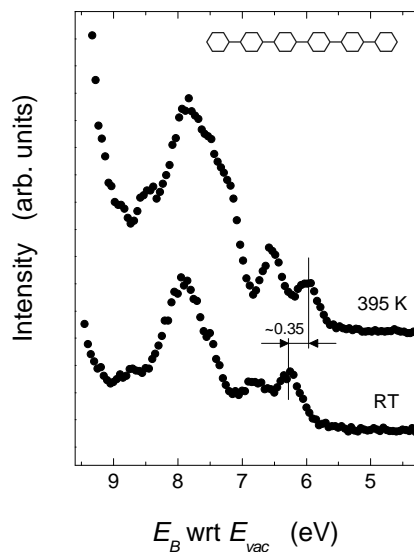


Fig. 3.1. The upper  $\pi$  bands of two sexiphenyl films with distinct ionization energies; the HOMO positions referred to the vacuum level are indicated by vertical ticks, their relative position identifies with the difference in ionization energies.

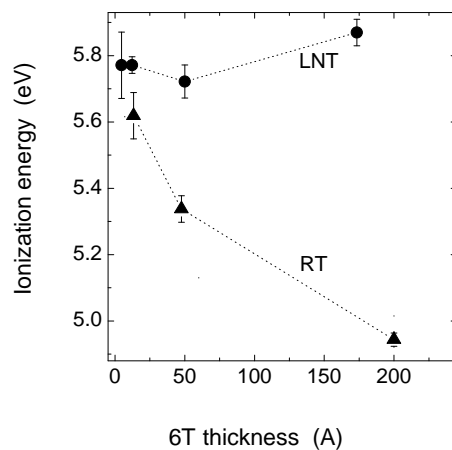


Fig. 3.2. The thickness dependence of the ionization energy of sexithiophene films grown on  $\text{SiO}_x$  at liquid nitrogen (LNT) and room temperature (RT).

about 0.8 eV suggesting gradual major changes in the electronic structure. The differences were presumably owing to the molecular order and the lack of it, as it occurs in the RT- and LNT-grown films (Ref. [27]). Similar trends were reported for the NADPO [62].

The variable  $E_I$  implies its importance for the characterization of molecular films, thus



the necessity of adhering to the vacuum level reference, and consequently—besides the BA evaluation—the need of the work function examination. If the characterization of the work function is neglected, the electronic distinctness of the molecular film can be unnoticed. In contrast to the habitually employed Fermi level reference, the vacuum-level reference eliminates rigid energy shift arising from the vacuum level changes and thereby enables the comparison of films grown on different substrates.

Further studies reported the ionization energy changes for 6T [27, 63], DH6T [63], and for rigid molecules, such as CuPc [64-66], F<sub>16</sub>CuPc [65], PEN [67], and PFP [58], too. Provided that the molecular orientation of grown film was examined, an evident relation between the ionization energy and the molecular orientation was revealed. Specifically, the following films and the corresponding  $\Delta E_I$ —when going from the lying towards the (nearly) upright molecular orientation—were reported: CuPc: -0.4 eV [65, 68]; 6T: -0.4 eV [63]; PEN: -0.55 eV [69]; DH6T: -0.6 eV [63]; F<sub>16</sub>CuPc: +0.7 eV [65, 68]; and PFP: +0.7 eV [70], +0.85 eV [69]. Note that both sign of changes were observed.

### 3.2 Work function, $\phi$

The work function of a free surface,  $\phi$ , has two contributions:

$$\phi = \mu_{bulk} + \phi_{SD}, \quad (3.1)$$

where  $\mu_{bulk}$  states for the internal (bulk) chemical potential and  $\phi_{SD}$  denotes the surface-dipole potential.

A particular material manifests its work function provided that the sufficient amount is probed. This is known for investigated inorganic (*e.g.* elemental) surfaces of films prepared on supported substrates, where the electronic properties of the substrate have to be eliminated and those of the overlayer developed. This is attained for film thicknesses exceeding a critical thickness [71]. The transition thickness range, accordingly the film thickness lower than the critical thickness, can span from a monolayer to multilayers and it was attributed to a violation of the local charge neutrality in films [72].

As for molecular films, the work function had been studied and mostly examined in the relation with the interfacial properties of the film/substrate interface. Specifically, the work function change,  $\Delta\phi_{subs}$ , upon the molecular film growth has been commonly examined:

$$\Delta\phi_{subs} = \phi_{subs} - \phi_{film} = \Delta E_{vac}, \quad (3.2)$$

for the vacuum level shift,  $\Delta E_{vac}$ , had been identified with a dipole formed at the film/substrate interface, the interfacial dipole (ID):

$$\Delta E_{vac} \equiv ID, \quad (3.3)$$

where  $\phi_{subs}$  is the work function of the pristine substrate surface, which changes to  $\phi_{film}$  upon the film growth. The ID affects the transport barrier for charge carriers injected across the junction. Figure 3.3 shows a typical  $\Delta\phi_{subs}$  upon the molecular film growth, namely of the Al(111) surface upon sexiphenyl growth with  $\Delta\phi_{subs} \approx 0.45$  eV. This *abrupt* change of the vacuum level—occurring within the completion of about one monolayer here—is considered to be a manifestation of the ID.

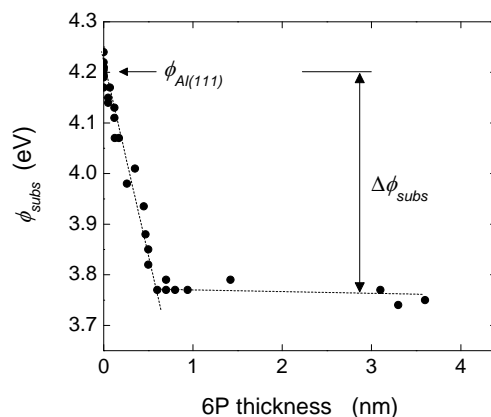


Fig. 3.3. The substrate work function change  $\Delta\phi_{subs}$  upon the sexiphenyl (6P) film growth.

In terms of the work function evolution upon the film growth, the research has been focused on the work function *change*, and not the work function *per se*; hence,  $\Delta\phi$  have been conceptually perceived as  $\Delta\phi_{subs}$  in Eq. (3.2), accordingly, the modified work function pertinent to the substrate. Yet, a sufficiently thick molecular film should display the work function relevant to the film itself likewise to films formed by inorganic electronic materials. Such work function is referred to as an intrinsic work function,  $\phi_{int}$ , throughout this study. It will be shown in the following that  $\phi_{int}$  both characteristic of the particular film and independent of the substrate can be detected. Similar to the work function of inorganic materials, the term ‘intrinsic’ is apparently abundant, yet it is employed in this study in relation with the molecular films for it would distinguish  $\phi_{int}$  being the material constant from the work function of *thin* films, *i.e.*  $\phi_{film}$  in Eq. (3.2), which can differ from  $\phi_{int}$  due to subcritical thickness of the molecular film. In spite of ample photoemission studies on the organic film growth, the usable data in the literature for the distinguishing the intrinsic work function of various molecular films are relatively scarce as studies on thinner films have been favoured owing to a focus on examination of the interfacial properties, such as the BA and ID determinations.

Conclusive examples supporting the notion on the intrinsic work function of molecular films based on compiled data are collected in Tab. 3.1. The data demonstrate that the film work function ( $\phi_{film}$ ) of a particular sufficiently thick ( $t_{film}$ ) film tends to converge to the specific value irrespective the substrate characterized by its  $\phi_{subs}$ . Thereby,  $\phi_{subs}$  has no effect on the resulting work function of the thick molecular film. For example, the 10 nm-thick NiPc films displayed the same work function of 4.0 eV, whether grown on Au or Ag polycrystalline substrates, accordingly in spite of the marked difference of 0.8 eV between  $\phi_{subs}$ 's being of 5.2 eV and 4.4 eV, respectively [73]. This suggests that  $\phi_{int}$  of NiPc is of about 4 eV. Likewise, the work function of 12.8-nm-thick PTCBI films displayed the same magnitude of about 4.5 eV irrespective the employed substrates, such as Au, Ag, or Mg [74]. A next example would be the 6T films with almost the same work function (spanning from 4.3 to 4.5 eV) in spite of the growth onto three distinct substrates with their work function ranging from 3.9 to 5.4 eV [75]. Further,  $\phi_{int}$  of PTCDA is assumed to be of 4.7 eV, as this was the work function of 12 nm-thick films grown on GaAs (100) substrates with different work functions ranging from 4.52 to 5.39 eV attained via

specific surface modifications [76].

The above mentioned and further examples are summarized in Tabs. 3.1 and 3.2, whilst Tab. 3.2 contains solitaire measurements, thus of thick particular films prepared on one kind of substrate. Admittedly, the latter examples do not rigorously prove that the particular film ends up with  $\phi_{int}$  irrespective of the substrate. Yet, the film thickness and the growth conditions suggest that  $\phi_{int}$  was attained. Rather large span of work functions can be noticed when various thick films of a particular molecule are compared, *e.g.* of 0.47 eV among the F<sub>16</sub>CuPcs and about 0.6 eV among 6Ts; the data are apparently scattered mostly owing to the varying molecular orientation. The issue on the molecular orientation-resolved  $\phi_{int}$  will be discussed below.

Of the numerous reported molecular films, eligibility of a particular film for the compilation resumed in Tabs. 3.1 and 3.2 was determined by the following concerns:

- (i) The sufficient film thickness: the molecular films with the thickness of 5-10 nm were adopted. Thinner films, but still moderately thick ones, were included in the compilation provided that work function was similar to the work function of the same thick film grown however on distinct substrates and substrate-related features in the spectra were absent.
- (ii) The growth fashion: nominally thick molecular films, yet with the detectable substrate features, were excluded, since this suggested electronically and morphologically markedly inhomogeneous films [58, 70, 77, 78].

The mentioned selection concerns applied on the variety of reported photoemission studies naturally limit the number of eligible data, which eventuates to the list of rather frequently investigated molecules. Note that the employed substrates include metallic, semiconducting, and molecular surfaces.

Tab. 3.1. The ionization energy,  $E_{I, film}$ , the work function,  $\phi_{film}$ , of thick molecular films with the thickness  $t_{film}$  grown on a variety of substrates described by their work function,  $\phi_{subs}$ . The indices  $L$  and  $U$  indicate the values relevant to the lying and upright geometry, respectively, provided that the molecular orientation was probed. The work function values, which were not explicitly reported in the literature, were calculated using the formula  $\phi = E_I - BA$ . The HOMO positions necessary for the  $E_I$  evaluation were determined according to their low- $E_B$  onsets. The UHV-SiO<sub>2</sub> states for the SiO<sub>2</sub> prepared under UHV conditions [27]. Further employed acronyms state as follows: PEDOT:PSS [Poly(3,4-ethylenedioxythiophene):poly(styrenesulfonate)], SAM (self-assembled monolayer), and HOPG (highly-ordered pyrolytic graphite).

Molecular film			Substrate		Ref.
Acronym	$t_{film}$ (nm)	$\phi_{film}$ (eV)	$E_{I, film}$ (eV)	Acronym	
6T	10	3.95 <sup>U</sup>	4.4 <sup>U</sup>	Native SiO <sub>2</sub>	4.26
	23	3.88 <sup>U</sup>	4.6 <sup>U</sup>		4.06
	5	4.35 <sup>L</sup>	5.35 <sup>L</sup>	SiO <sub>2</sub> (90K)	4.83
	20	3.96 <sup>U</sup>	4.65 <sup>U</sup>	Si(111)-7×7	4.6
	20	3.94 <sup>U</sup>	4.55 <sup>U</sup>	UHV-SiO <sub>2</sub>	5.05
	30	3.97 <sup>U</sup>	4.7 <sup>U</sup>		5.15

Tab. 3.1 *continued*

6T	2.8	4.3	5.3	Au	5.1	[75]
	5.2	4.5 <sup>L</sup>	5.15 <sup>L</sup>	Au/PFDT	5.4	
	5.3	4.3	5.2	Au/ODT	3.9	
	6.4	3.5	5.3	Ag	4.2	[79]
	2-3	3.9	4.6	Pd	5.1	
	2-3	4.0	5.2	Au	5.2	
	2-3	4.0	4.6	Pt	5.5	
	2-3	3.8	4.5	Contaminated Ag	4.0	
	2-3	3.9	4.4	Contaminated Pd	4.4	
	2-3	3.9	4.4	Contaminated Au	4.3	
	2-3	4.0	4.5	Contaminated Pt	4.1	
$\alpha$ -NPD, NPB	5.5	3.8	5.2	Au/Alq <sub>3</sub>	4.0	[80]
	10	3.95	5.35	Au	5.1	[81]
	10	4.18	5.4	Au	5.14	[82]
	10	3.4	5.5	Mg	3.65	
BCP	10	4.18	6.4	Au/ $\alpha$ -NPD	4.18	
	n.a.	4.14	6.4	Au/doped $\alpha$ -NPD	4.74	
	n.a.	3.4	6.4	Mg/ $\alpha$ -NPD	3.4	
BP2T	25.6	4.47	5.3	Au/F <sub>16</sub> CuPc	4.8	[83]
	20	4.71	5.27	Au	5.3	
CBP	10	4.45	6.21	Au/ZnPc	4.45	[82]
	10	4.54	6.16	Au/doped ZnPc	5.04	
CuPc	5-10	3.9	5.0	Au	5.3	[84]
	9.4	4.1	5.0	Au(100), Au	5.3	[85,86]
	11	4.1	5.0	GeS(100)	4.6	[86]
	15	3.87	4.82	<i>p</i> -Si(111)	4.22	[20]
	5	4.35 <sup>L</sup>	5.2 <sup>L</sup>	HOPG	n.a.	[65]
	5	3.95 <sup>U</sup>	4.8 <sup>U</sup>	SiO <sub>2</sub>	n.a.	
	20	4.24	4.82	Native SiO <sub>2</sub> /F <sub>16</sub> CuPc	5.3	[87]
	3.6	4.0	4.6	H-Si(111)	4.28	[39]
F <sub>4</sub> CuPc	9	3.9	5.0	Au	5.3	[84]
	5-10	4.7	5.7	Au	5.3	
	5-10	4.3	5.7	ITO	4.2	
	8.5	4.7	5.7	Au(100)	5.3	
F <sub>16</sub> CuPc	15	4.7	5.55	<i>p</i> -Si(111)	4.22	[20]
	9	4.95	6.1	Au	5.3	[84]
	15	5.42	6.32	<i>p</i> -Si(111)	4.22	[20]
	25.6	5.13	6.44	Au/BP2T	4.71	[83]
	20	5.3	6.66	Native SiO <sub>2</sub> /CuPc	4.24	[87]
	10	5.1	6.3	Au	5.0	[88]
	4	4.7 <sup>L</sup>	5.9 <sup>L</sup>	HOPG	4.3	[65]
4	5.3 <sup>U</sup>	6.6 <sup>U</sup>	Au(111)/C <sub>8</sub> -SAM	n.a.		

Tab. 3.1 *continued*

HAT-CN	90	5.95	9.75	ITO	4.46	[89]
	80	6.1	9.9	Au	5.2	[90]
NiPc	10	4.0	5.0	Au	5.2	[73]
	10	4.0	5.0	Ag	4.4	
PEN	6.4	4.33	4.91	SiO <sub>2</sub>	4.33	[91]
	15	4.35	5.2	Au	5.4	[81]
	12.8	4.5	4.85	PEDOT:PSS	5.3	[92]
	20	4.32 <sup>U</sup>	4.77 <sup>U</sup>	SiO <sub>2</sub>	n.a.	[67]
	3.2	4.47 <sup>U</sup>	4.73 <sup>U</sup>	HOPG/CuPc	n.a.	
PFP	7	4.95	5.6 <sup>L</sup>	Au(111)	5.45	[70]
	7	4.95	~6.3 <sup>U</sup>	Au(111)	5.45	
PTCBI	12.8	4.6	6.2	Au	5.0	[74]
	6.3	4.5	6.2	Ag	4.3	
	6.3	4.5	6.0	Mg	3.8	
PTCDA	12	4.77	6.67	GaAs(100)-c(4×4)	4.63	[76]
	12	4.56	6.6	S-GaAs(100)	4.52	
	12	4.55	6.58	S-GaAs(100)	4.68	
	12	4.65	6.56	S-GaAs(100)	4.98	
	15	4.94	6.95	S-GaAs(100)	5.4	[20]
	12	4.8	6.65	Se-GaAs(100)-(2×1)	5.39	[76]
	10	5.0	6.8	Au	5.2	[93]
	8	4.8	6.55	HOPG/F <sub>16</sub> CuPc <sup>L</sup>	4.7	[65]
8	4.95	6.4	C <sub>8</sub> -SAM/F <sub>16</sub> CuPc <sup>U</sup>	5.3		

Tab. 3.2. The continuation of Tab. 3.1 but for molecular films with only solitary reported growth on a particular substrate.

Molecular film				Substrate		Ref.
Acronym	$t_{film}$ (nm)	$\phi_{film}$ (eV)	$E_{I,film}$ (eV)	Acronym	$\phi_{subs}$ (eV)	
6P	20	4.3	6.1	Au	5.1	[81]
Alq <sub>3</sub>	15	4.0	5.7	Au	n.a.	[80]
DH4T	10.4	4.05 <sup>U</sup>	4.9	Au	5.25	[94]
DH6T	6	~ 3.6	4.85	Ag(111)	4.5	[45]
DiMe-PTCDI	15	4.55	6.58	S-GaAs(100)	5.17	[20]
H <sub>2</sub> Pc	15	4.04	4.96	<i>p</i> -Si(111)	4.22	[20]
PTCDI	15	4.67	6.42	S-GaAs(100)	5.28	[20]
ZnPc	10	4.45	5.29	Au	5.14	[82]

### 3.2.1 Molecular orientation-resolved intrinsic work function.

The work function comprises of two contributions, namely of the chemical potential and the surface dipole [Eq. (3.1)]. The latter depends on the molecular orientation, since different molecular orientations imply the distinct surface terminations leading to the different surface dipole. Therefore, it is reasonable to presume that the intrinsic work function of a particular molecular film depends on the molecular orientation in the surface region. Two extreme situations in terms of the molecular orientation can occur: the film formed by lying- and upright-oriented molecules with the corresponding intrinsic work function, namely  $\phi_{int,L}$  and  $\phi_{int,U}$ . Thus, the molecular orientation-resolved work function of a particular molecular film would represent the work functions of the corresponding faces of a molecular crystal.

It can be noted that various surface reconstruction of single-crystal elemental surfaces can manifest the work function differing as much as several tenths of electronvolts. An extreme example would be the work functions of W(111) and W(110) being of 4.47 and 5.25 eV, respectively, thereby differing by 0.78 eV [95].

Given the data presented in Tab. 3.1 and 3.2, estimations on intrinsic work functions of selected molecular films are compiled in Tab. 3.3. Admittedly, the available data present a small statistical ensemble not sufficient for reliable estimates; nevertheless, the presented values are

Tab. 3.3. The estimated intrinsic work function  $\phi_{int}$  of selected molecular films discriminated by the molecular orientation. The values typed in bold were adopted from studies, where both work-function and molecular-orientation characterizations were performed. The remaining values were reported in works with lacking characterization of the molecular orientation; yet both the film thickness and the growth conditions suggest the upright-oriented molecules.

Molecular film	$\phi_{int,L}$ (eV)	$\phi_{int,U}$ (eV)
6T	~ <b>4.35</b>	~ <b>3.95</b>
$\alpha$ -NPD, NPB	–	3.8-4.2
Alq3	–	~ 4.0
BCP	–	~ 4.15
BP2T	–	4.5-4.7
CBP	–	~ 4.5
CuPc	~ <b>4.4</b>	~ <b>3.95</b>
DH4T	–	~ <b>4.05</b>
DiMe-PTCDI	–	~ 4.55
F <sub>4</sub> CuPc	–	4.7
F <sub>16</sub> CuPc	<b>4.7</b>	<b>5.3</b>
H <sub>2</sub> Pc	–	~ 4.0
NiPc	–	4.0
PEN	–	<b>4.3-4.5</b>
PFP	~ 4.95	~ 4.95
PTCBI	–	4.5-4.6
PTCDA	<b>4.5-4.94</b>	–
PTCDI	–	~ 4.7

intended to provide an aid for their further verifications. Note that the following molecular films show about the same  $\phi_{int} \sim 4.0$  eV for upright geometry: 6T [27, 79], 6P [96], H<sub>2</sub>Pc [20], CuPc [20, 39, 84], NiPc [73], Alq<sub>3</sub> [91],  $\alpha$ -NPD [82], and BCP [82]; we assume that the similar  $\phi_{int}$  are owing to similar surface terminations, namely carbon atoms with bonded hydrogen suggesting the similar surface dipole.

As it was mentioned above, thick films can undergo the L→U orientational transition (Fig. 2.1), which depends on the growth conditions such as the substrate surface morphology, growth rate, and growth temperature. This implies that the work function switches from  $\phi_{int,L}$  to  $\phi_{int,U}$  with the film thickness and the orientational transition-related work function change is

$$\Delta\phi_{L\rightarrow U} = \phi_{int,L} - \phi_{int,U}. \quad (3.4)$$

The orientational transition can be abrupt with the first lying monolayer followed by upright-oriented next monolayers [43-45, 98, 99]. Yet, the gradual transition accomplished up to thickness of several nanometres had been more frequently encountered [27, 39, 46-49, 100]. As the molecular orientation had been rarely determined in reported studies, the compilation presented in Tabs. 3.1 and 3.2 focussed to the molecular films with the thickness of 5-10 nm, where the L→U orientational transitions were presumably accomplished. Admittedly, the minimal thickness required for attainment of  $\phi_{int}$  may be substantially lower provided that the particular molecular orientation is preserved through the entire film.

In fact, the  $\Delta\phi_{L\rightarrow U}$  can be inferred from several studies, where thicker films were examined, yet with lacking molecular-orientation characterization: with the increasing film thickness, the work function suggests its saturation after the ID formation, but the work function continues to gradually drop by several tenths of electronvolts with the further growth. Such evolution was observed for 6T [27], NiPc [73], CuPc [39, 66, 86, 101, 102], and thiophene [75], and DH4T [94]. Yamane *et al.* suggested that the gradual work function change is due to the summation of incremental dipoles, which were arising due to the gradually changed molecular tilt angle [101].

Chen *et al.* measured simultaneously both the work function and the molecular orientation of CuPc films and observed the work function of 4.35 eV and 3.95 eV, *i.e.*, differing by -0.4 eV, for the films built from lying- and upright-oriented molecules [103]. Interestingly, the  $\Delta\phi_{L\rightarrow U} \approx -0.4$  eV, when going from lying- towards upright-oriented molecules, had been frequently observed for unsubstituted (hydrogen terminated) molecules, such as 6T [27, 63], NiPc [73], CuPc [66, 86, 101, 103-104], DH4T [94], HBC [49], DH6T [45]. In contrast,  $\Delta\phi_{L\rightarrow U} > 0$  was observed for fluorine-substituted molecular films such as F<sub>16</sub>CuPc (+0.85 eV) [103] (+0.6 eV) [65], and PFP [58]. Since fluorine has a high  $E_I$ , which in turn suggests the high work function of fluorine-terminated surface (see Section 3.4), the inequality  $\phi_L < \phi_U$  for the fluorine-substituted molecules can be qualitatively explained via the increased density of fluorine atoms terminating the film comprising upright oriented molecules in comparison to the film terminated by lying molecules.

### 3.3 Molecular orientation-resolved growth modes

Growth fashions of grown films are commonly categorized into three basic modes according to the morphology evolution, namely the Frank-Van der Merwe, Stranski-Krastanov, and Volmer-Weber growth modes referring to the laminar growth, the islanding on a wetting layer, and the island growth, respectively. The growth fashion determines the evolution of the probed surface

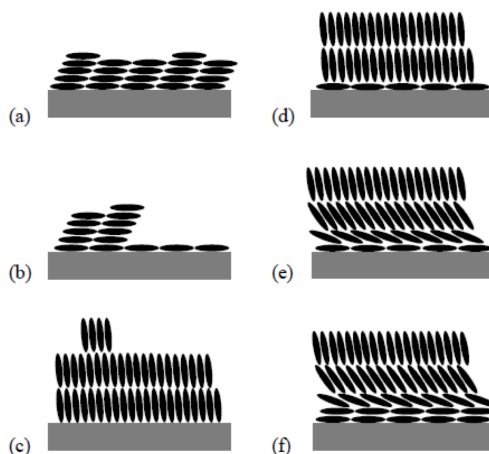


Fig. 3.4. The sketches of the often observed growth fashions of molecular films with the consideration of the molecular orientation. Except the panel (b) indicating the Stranski-Krastanov growth mode with the lying molecular orientation, all panels depict the lamellar growth, albeit with distinct evolutions of the molecular orientational transition. Reprinted with permission from J. Ivanco, *Thin Solid Films* **520** (2012) 3975. Copyright 2012 Elsevier.

electronic properties and, conversely, the evolution of electronic properties can be employed for the growth mode determination. For the surface electronic properties of molecular films are dramatically affected by the molecular orientation that has to be involved in the discernment of the growth fashions. Figure 3.4 illustrates the often observed growth fashions of molecular films with the consideration of the molecular orientation:

- (a) the lamellar growth of lying molecules;
- (b) the Stranski-Krastanov growth of lying molecules;
- (c) the lamellar growth of upright-oriented molecules;
- (d) the lamellar growth with the abrupt L→U orientational transition beyond the first lying monolayer;
- (e) the lamellar growth with the gradual L→U orientational transition beyond the first lying monolayer; and
- (f) the lamellar growth of a multilayer formed by lying molecules followed by the gradual L→U orientational transition.

Except the (b) representing the islanding, the further examples pertain to the lamellar growth. The (a – c) presume the molecular orientation preserved during the growth, the (d – f) consider the orientational transition. Note that the growth fashions illustrated in Fig. 3.4 are rather elementary ones chosen to illustrate possible scenarios. In reality, the structure evolution with the film thickness may be more complex particularly at a heterostructure growth [105].



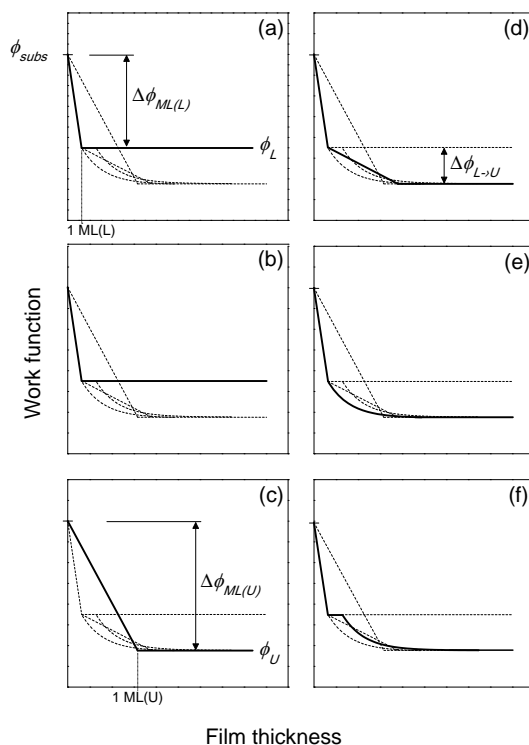


Fig. 3.5. The sketched work function evolutions—and thereby the energy level shift—with the film thickness corresponding to the distinct growth scenarios shown in Fig. 3.4 are indicated by thick solid lines. Besides, all discussed  $\phi$ -evolutions are repeatedly drawn by dashed lines in each panel to allow the comparison. The more frequent encountered inequality  $\phi_L > \phi_U$  was assumed here. The  $\Delta\phi_{ML(L)}$  and  $\Delta\phi_{ML(U)}$  refer to the  $\Delta\phi$  examined upon the growth of 1<sup>st</sup> monolayer formed by lying- and upright-oriented molecules, respectively. Reprinted with permission from J. Ivanco, *Thin Solid Films* **520** (2012) 3975. Copyright 2012 Elsevier.

As for the work function change,  $\Delta\phi$ , induced by the molecular film growth, two contributions can be distinguished; namely due to (1) the formation of the 1<sup>st</sup> monolayer,  $\Delta\phi_{ML}$ , accounted for the ID formation, and (2) the L $\rightarrow$ U orientational transition,  $\Delta\phi_{L\rightarrow U}$  [Eq. (3.4)]:

$$\Delta\phi = \Delta\phi_{ML} + \Delta\phi_{L\rightarrow U}, \quad (3.5)$$

Panel *f* shows a scenario with the  $\Delta\phi_{L\rightarrow U}$  occurring at higher film thickness, which is manifested by an intermediate flattening of the work function at small thickness. The plateaued work function may suggest further examinations at higher thickness redundant. The work-function plateau can be absent provided that molecules are exclusively oriented upright through the entire film (panel *c*), *i.e.* including the first monolayer, or the abrupt change from the lying towards upright occurs when going from the first to second monolayer (panel *d*) [45, 98, 99]. Note, that only the scenarios (*a-c*) correspond to the expected work-function change illustrated in Fig. 3.3. The situations (*d-f*) representing the orientational transitions had frequently implied erroneous

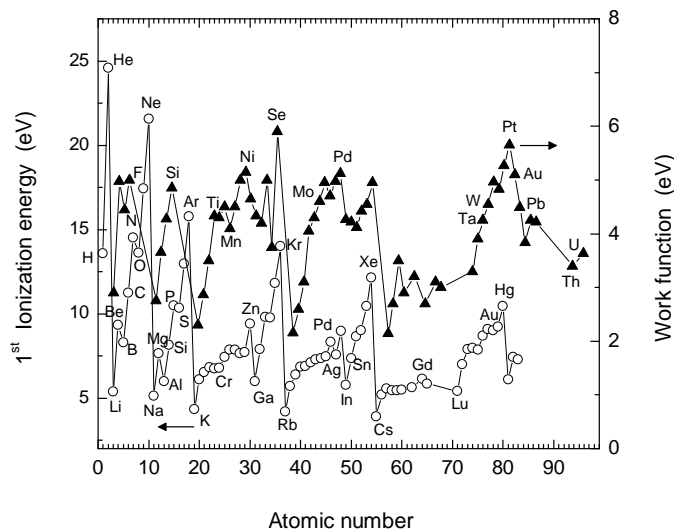


Fig. 3.6. The first ionization energy of elements (empty circles, [95]) suggests the correlation with the work function (full triangles, [108]) of corresponding surfaces. The solid line connecting the data points are to guide the eye. The arrows indicate the relevant coordinate.

conclusions on the presence of a band bending (*e.g.* Refs. [98, 99]), the situation ( $\epsilon$ ) was rationalized as the mixing the interfacial dipole and a band bending [106]; the issue will be discussed in more details in Section 3.5.

### 3.4 The ionization energy-work function correlation

In a first approximation, the first ionization energy of elements and the work function of the corresponding surfaces are correlated [107]: the correlation plot is shown in Fig. 3.6 with  $E_I$  and  $\phi$  values adopted from Refs. [95] and [108]. So far as distinct surface reconstructions for a particular element are reported, the magnitude for the unreconstructed surface was assumed.

Analogous to the  $\phi$ - $E_I$  correlation for elements (Fig. 3.6), the thick molecular films show the  $\phi_{int}$ - $E_I$  correlation too. This is shown in Fig. 3.7a, where the  $\phi_{int}$ - $E_I$  points of molecular films (empty circles, adopted from Tab. 3.1) and the replotted correlation graph for elements introduced in Fig. 3.6 (full circles) are juxtaposed. Figure 3.7b repeats the  $\phi_{int}$ - $E_I$  correlation for molecular films though with their assignment. The dashed lines represent the corresponding linear fits, whilst As, C, and Hg—the merely labelled elements in the graph—were retracted from the fitting due to their large deviation. The linear fits follow the equations:

$$\phi_{el} = 0.08 + 0.56 \times E_{I,el} \quad (3.6)$$

$$\phi_{int} = 2.1 + 0.41 \times E_{I,org} \quad (3.7)$$

for the elements and for the molecular films addressed in this work. Note that the dispersion of the  $\phi_{int}$ - $E_I$  dependences for both molecular films and elements are comparable. The correlation plot for molecular films does not discriminate the molecular orientation as there is a shortage

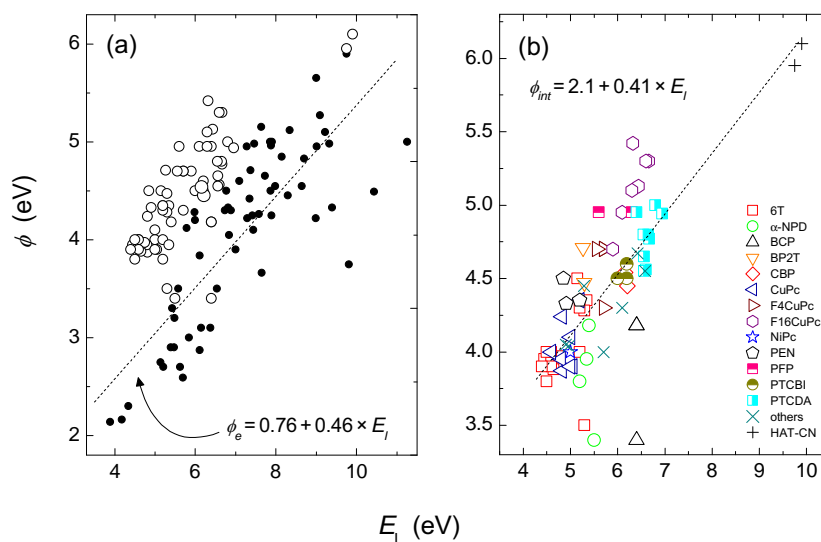


Fig. 3.7. (a) The  $\phi$ - $E_I$  correlation for elemental surfaces (full circles, [95, 107, 108]) and for surfaces of oligomeric molecular films addressed in this work (empty circles), (b) the  $\phi_{int}$ - $E_I$  correlation for molecular films replotted from panel (a) with indications of particular molecules.

of data explicitly relating the work function and the molecular orientation for specific organics. Note that the correlation suggests the commensurably high  $\phi_{int}$  of the films with high  $E_I$ , such as TCNQ,  $F_4$ TCNQ,  $F_4$ CuPc,  $F_{16}$ CuPc, NTCDA, and HAT-CN.

### 3.5 Band bending deduction from photoemission

The free charge carrier concentration in the subsurface region of a semiconductor can be controlled by a field effect, *i.e.* altering the electron energy levels by an external field. The effect is also termed the band bending as the energy bands change their relative position with respect to the Fermi level in the subsurface region. Both the upward and downward band bending can occur, the former being illustrated in Fig. 3.8. In contrast to *e.g.* metals, where the binding energies of core levels  $E_B$  are constant,  $E_B$  of semiconductors core levels depend on the doping level, as that determines the position of the Fermi level in the energy gap. The band bending implies the shift of photoemission features for those are determined with respect to the analyser ground, so to the Fermi level. Conversely, the energy difference between the core levels at a semiconductor surface and in the bulk assigns the band bending. The upward-bent bands result in the high- $E_B$  rigid shift of all levels with the depth in semiconductor, accordingly away from the Fermi level; this is shown in Fig. 3.8 for the valence band edge. The band bending is caused by an external field or by a surface/interface charge and—conversely—the latter can be determined, *e.g.*, by examination the core-level shift upon an external bias [109].

In organic electronics, some concepts well established in inorganic semiconductors, *e.g.* the band bending, had been adopted for the molecular films. The presence of the band bending in molecular films would be of great importance for organic FETs; it would mean that the underly-

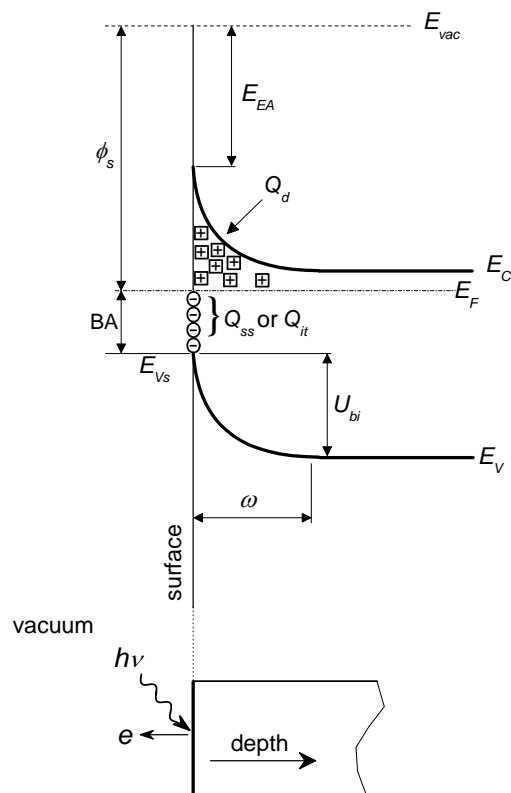


Fig. 3.8. The energy diagram of  $n$ -type semiconductor with the upward band bending;  $\phi_s$  is the semiconductor work function,  $E_{EA}$  is the electron affinity at the surface,  $Q_d$  is the depletion zone charge,  $w$  is the depletion zone width,  $U_{bi}$  is the built-in potential identified with the band bending magnitude, and the BA is the band alignment, i.e. the binding energy of the valence band edge on the surface,  $E_{Vs}$ .  $Q_{ss}$  and  $Q_{it}$  are the charge in surface and/or interface states, respectively. The bottom pictogram sketches the experimental set up.

ing operational mechanism of OFET mimics that of the traditional (inorganic) FET. Therefore, the issue had been carefully followed in photoemission characterizations of molecular films; the conclusion on upward band bending had been habitually allured by observing the high- $E_B$  shift of photoemission features with increasing film thickness [73, 74, 77, 80, 83, 86, 87, 106, 110-115]. The downward band bending was reported in  $F_{16}CuPc$  [116]. One should recognize that the high- $E_B$  shift associated with the band bending is an additional, further shift to that induced by the interfacial dipole (ID); the ID-related shift is abrupt; it is manifested by the work function drop, which commonly saturates within the completion of about a monolayer (Fig. 3.3). On the other side, the band-bending-associated shift is the gradual one in the range of several nanometres. The band bending in organic materials supposedly occurs owing to a light doping induced by impurities derivable from synthesis.

The prevailing notion on the (upward) band bending in a molecular film is explained in

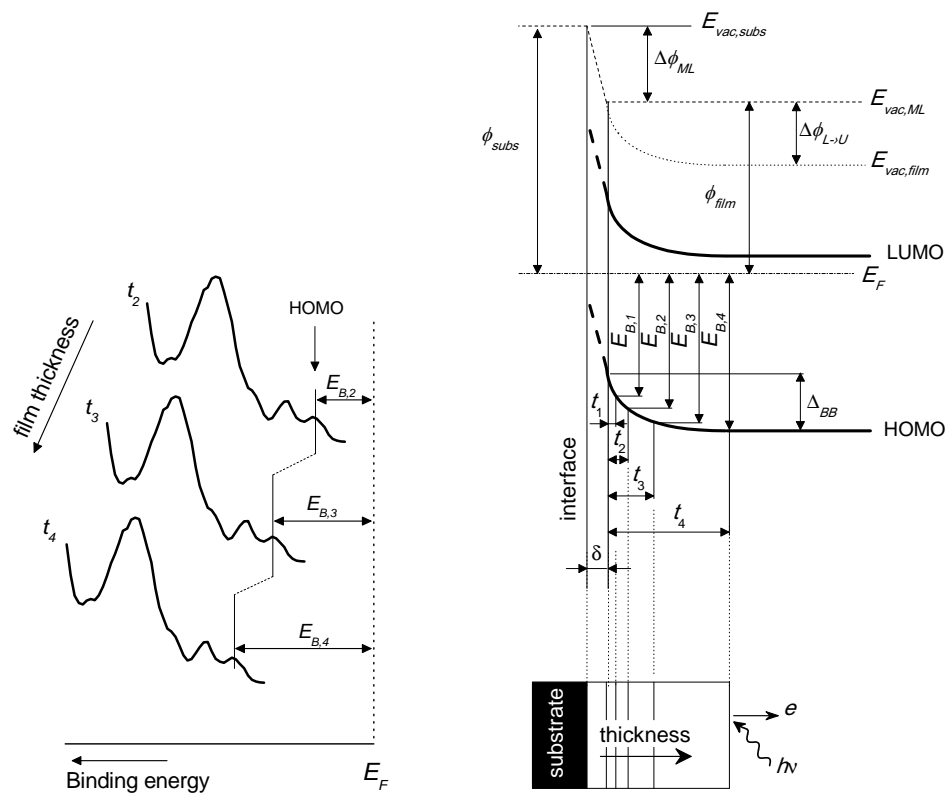


Fig. 3.9. The high-binding energy shift of energy levels with the increasing film thickness,  $t_2 < t_3 < t_4$  (left panel) and the corresponding notion in terms of the band bending in the grown molecular film (right panel). The  $t_1$  is the thickness of the first monolayer. The pictogram sketches the experimental set up.

Fig. 3.9; the left panel shows the high- $E_B$  shift of VBs of a molecular film with the increasing film thickness,  $t_2 < t_3 < t_4$ . The right panel transforms the varying particular HOMO positions,  $E_{B,2} < E_{B,3} < E_{B,4}$ , to the corresponding points in the energy band diagram suggesting the band bending. The  $E_{vac,ML}$  is the vacuum level upon the formation of the first monolayer with the thickness  $\delta$ ,  $\Delta\phi_{ML}$  is the corresponding vacuum-level change identified with the interfacial dipole. The  $\Delta_{BB}$  is the total shift of energy levels of the film beyond the first monolayer interpreted as the band bending.

The above interpretation framework presumes that the situation introduced in Fig. 3.9 is equivalent to the detection of the band bending at the surface or interface of inorganic semiconductors (Fig. 3.8). Yet, there is an essential difference as far as the respective photoemission characterizations are concerned; whereas the band bending in inorganic semiconductors is examined by a single measurement, the band bending in molecular films is deduced from a series of sequentially performed measurements during the film growth (see sketches at the bottom of the Fig. 3.8 and Fig. 3.9). The most importantly, the successive characterizations of the molecular film are performed at distinct conditions, namely, at varying work function, which itself affects

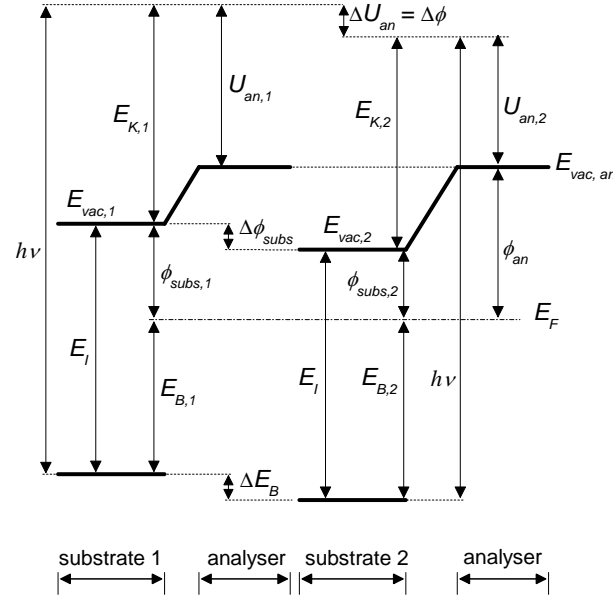


Fig. 3.10. The principal energy diagram of the photoemission measurement contrasting an adsorbate characterized by its ionization energy on surfaces with work function  $\phi_{subs,1}$  and  $\phi_{subs,2}$  (see text).

the shift of binding energies employed for the conclusions on the band bending. In other words, the interpretation framework for the band bending tacitly presumes the constant vacuum level after the first ML formation,  $E_{vac,ML}$ , with the increasing film thickness (Fig. 3.9 right panel, dashed line). Instead, the vacuum level varies according to  $E_{vac,film}$  (dotted line) owing to the L→U orientational transition, thereby differing by  $\Delta\phi_{L\rightarrow U}(t)$  from  $E_{vac,ML}$ . In the next paragraph, it will be shown that the work function change itself of the probed surface results in the equal rigid shift of photoemission spectra.

In probing the photoemission process, the binding energy,  $E_B$ , of a core level is given by the equation [117]:

$$E_B = h\nu - U_{an} - \phi_{an}, \quad (3.8)$$

where  $h\nu$  is the photon energy,  $U_{an}$  is the voltage applied to the analyzer to detect an emitted electron, and  $\phi_{an}$  is the work function of energy analyzer.  $E_B$  is referred to the Fermi level. Even though Eq. (3.8) does not explicitly involve the work function of the substrate, this affects the binding energy  $E_B$  of an adsorbate. This is shown in Fig. 3.10, where the principal energy diagrams for the photoemission characterization of a particular atom, yet adsorbed on two electronically distinct substrates, are contrasted: the substrates are described by their work functions,  $\phi_{subs,1}$  and  $\phi_{subs,2}$ , the adsorbate is detected via its core level with the binding energy  $E_B$ . Since the ionization energy of the adsorbate  $E_I$ —being a sum of  $E_B$  and substrate work function  $\phi_{subs}$ —is constant on both substrates, the analyzer detects  $\Delta E_B = E_{B,2} - E_{B,1}$  equal to the substrate work function difference,  $\Delta\phi_{subs} = \phi_{subs,1} - \phi_{subs,2}$  [118].

The high- $E_B$  shift in thicker films (which is regarded as the band bending) and the work

function drop are yoked effects and they virtually occur upon the first monolayer formation too: the molecule photoemission features shift towards high  $E_B$  simultaneously with the work function drop with the film thickness at submonolayer coverages. Consequently, the shift of photoemission spectra, either upon the growth of first monolayer or with further increase of the film thickness, has a common nature, namely the work function change of the probed surface.

Ref. [119] provides plausible examples demonstrating the influence of the substrate work function on the photoemission spectra; photoemission spectra of ZnTPP grown on various metal (Mg, Ag, Au, Al) substrates shifted upon the oxygen exposure by amount equal to the expected work function changes due to the oxidation of the corresponding substrate. Likewise, the photoemission spectra of bithiophene were aligned according to local substrate work function on nanoscopically patterned surfaces [120].

As for the origin of the work-function change inducing the shift of the photoemission spectra, this is commonly caused by the L→U orientational transition occurring in thick molecular films (Fig. 3.5), though the oxidation can be at play too [115]. Upon the growth, the adsorbed molecules successively build particular monolayers, while the  $n$ th monolayer represents a substrate for the  $(n + 1)$ th monolayer. Due to molecular orientation-resolved work function, the gradual L→U orientational transition with the film thickness implies the concomitant and incremental work function change. Accordingly, the photoemission spectra of  $(n + 1)$ th molecular layer will be rigidly shifted relative to the spectra of the  $n$ th layer by their work function difference. The summed shift corresponds to the total work function change due to the L→U orientational transition  $\Delta\phi_{L\rightarrow U}$  [Eq. (3.4)], which is identical to  $\Delta_{BB}$  (see Fig. 3.9). Consequently, the shift of photoemission features with the film thickness considered to imply the band bending is, in fact, due to  $\Delta\phi_{L\rightarrow U}$  induced by the gradual L→U orientational transition. In other words, the high- $E_B$  (low- $E_B$ ) shift accompanied by the same work function drop (increase) does not implicate any band bending. The spectra shift  $\Delta E_B$  would indicate the factual band bending provided that the shift exceeds the work function change; in such a case, the difference would indicate the band bending:

$$\Delta E_B - \Delta\phi_{L\rightarrow U} = \Delta_{BB}. \quad (3.9)$$

The spurious band bending can be recognized also at the organic-organic interfaces. This can be illustrated on CuPc/CuPcF<sub>16</sub> and F<sub>16</sub>CuPc/CuPc heterostructures [87], so prepared by both deposition sequences; the F<sub>16</sub>CuPc-related features shifted towards low  $E_B$  with the F<sub>16</sub>CuPc growth onto CuPc, while the growth of CuPc over CuPcF<sub>16</sub> resulted in the high- $E_B$  shift of the CuPc spectra. The low- and high- $E_B$  shifts were interpreted as the downward and upward band bending, respectively and the depletion/accumulation region of about 15 nm gave to an estimate of the free charge carrier concentration of about  $10^{18} \text{ cm}^{-3}$ . With reference to the discussion above, we presume that the would-be band bending in Ref. [87] is an artefact induced by the varying work function: The intrinsic work function of CuPc and F<sub>16</sub>CuPc for lying (upright) films are 4.4 (3.95) and 4.7 (5.3) eV, respectively (Tab. 3.1). Therefore, the work function upon the growth of CuPc onto F<sub>16</sub>CuPc converges to  $\phi_{CuPc}$  (accordingly, it drops) and thereby implicates the high- $E_B$  shift. The opposite situation occurs for the reversed growth sequence, namely the work function increase towards the intrinsic value of F<sub>16</sub>CuPc and thereby the low- $E_B$  shift. Depending on the molecular orientation of CuPc and F<sub>16</sub>CuPc, and the growth sequence, the total work-function change ranges between 0.3 to 1.35 eV. The qualitatively same situation was observed for F<sub>16</sub>CuPc/BP2T and BP2T/F<sub>16</sub>CuPc organic heterostructures [83].

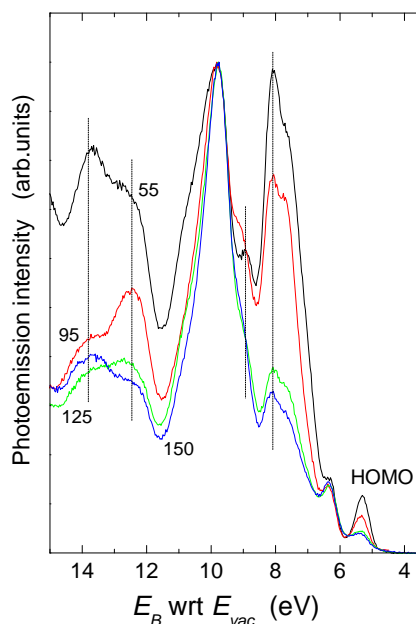


Fig. 3.11. The valence band spectra of the CuPc film examined at photon energies of 55, 95, 125, and 150 eV and normalized with respect to the dominant peak. Reprinted with permission from T. Toader *et al.*, Phys. Stat. Sol. (b) **246** (2009) 1510. Copyright 2009, John Wiley & Sons, Inc.

### 3.6 $\pi$ band

Unlike the isolated and thereby well-identifiable core levels, the shallow levels determining the electronic structure of an organic molecule are markedly affected by the band dispersion and intramolecular interactions. Many vaguely identified, narrowly distributed and to various extents overlapped molecular orbitals populate the sub-Fermi region to eventually form the (valence) band (recall Fig. 1.2), also referred to the density of states (DOS). Apart from the band alignment determination, *i.e.* the examinations of the HOMO positions with respect to the Fermi level, the rest of the valence band has been rather scarcely examined experimentally [121-123] thereby providing a weak feedback to *ab initio* calculations of the molecular electronic structure [124, 125].

Employment of the tunable photon energy in the photoemission characterization allows in some extent to specify the character of particular molecular orbitals, accordingly their assignment to constituting atoms of a molecule. The approach is viable for assemblies comprising elements with distinct photoionization cross section (PCS) dependences on photon energy; the marked differences can be encountered between *e.g.* carbon and metallic elements [16]. Thus, by monitoring intensities of particular molecular orbitals in dependence of the photon energy, the orbitals can be discriminated in terms of their character.

Figure 3.11 shows normalized VB spectra of CuPc ( $C_{32}H_{16}CuN_8$ ) probed with various photon energies. By knowing the ratio between the photoionization cross sections of Cu 3d, C 2p,



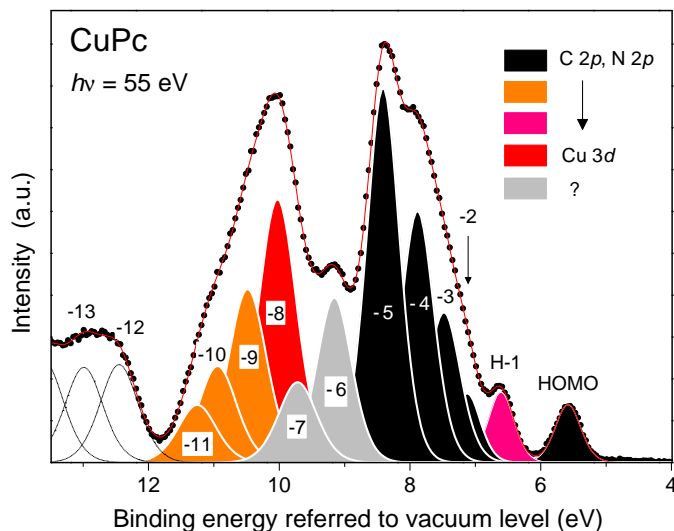


Fig. 3.12. The deconvoluted valence band of CuPc: The characters of particular molecular orbitals ranging from entirely Cu 3d-derived to entirely C 2p or N 2p-derived energy levels are indicated. The particular orbitals are numbered with respect to the HOMO. Reprinted with permission from T. Toader *et al.*, Phys. Stat. Sol. (b) **246** (2009) 1510. Copyright 2009, John Wiley & Sons, Inc.

and N 2p energy levels and relative intensities of individual orbitals in dependence of the photon energy, the character of particular orbitals can be deduced. Figure 3.12 shows individual molecular orbitals obtained by the deconvolution with the indication of their character spanning from the C 2p- and N 2p-derived (which are not distinguishable by this method owing to their very similar PCS photon energy dependences) to the Cu 3d-derived orbitals. The notable result would be the experimental confirmation of the pure C 2p-character of the HOMO, of which dissonant characters were suggested by theoretical investigations [124, 125].

#### 4 Interfaces associated with molecular films

The interfaces are—besides the active films—the functional parts of electronic devices. The interface engineering aims to control interfacial electronic properties (energy level alignment determining the injection/extraction barriers), chemistry, and morphology. In terms of electronic properties, organic electronics has, in fact, introduced a novel class of interfaces, namely these formed between molecular films and metals or inorganic semiconductors. In organic devices, matched pairs of materials are necessary to conduct away charges across junctions on metal/organic interfaces or to separate charges at organic acceptor/donor interfaces. As for the latter class of interfaces, the interest had been nourished due to organic heterostructures, which have become an integral part of organic devices based on a double layer or a bulk heterostructure. In spite of conclusive success of organic devices, the ability to predict and control the electronic properties of interfaces has been limited.

Conductive contacts in organic devices have been regularly realized by means of metals. Among the most relevant ones were the coin metals such as *e.g.* Ag, Al, Au, Cu, Ni, Pt, Sn, Zn. The metallic contact to the molecular film can be accomplished either by the growth of a molecular film on a metallic substrate/film or—reversely—by the evaporation of a metal onto a molecular film. In practise, the former interface has been studied via the growth of an organic layer prevailing on both chemically and structurally well-controlled inorganic substrates, typically of single-crystal surfaces, whereas the latter interface (the reverse one) through the evaporation of a metal onto an organic film.

The evaporated molecules have virtually no morphological effect on the metallic substrate and such interfaces are sharp with the topology determined by the substrate surface, and they can even manifest an epitaxial relation between the film and the substrate. Therefore, they allow more straightforward analysis and interpretation of interface properties, and particularly electronic interfacial properties have been conveniently studied via organic-on-metal contacts simply because of higher reproducibility, characterization, and overall control of the interface compared to the reversed interfaces.

The metal evaporation onto organic surface may be more invasive to the organic substrate. The higher heat of adsorption of metal atoms can increase their reactivity and result in chemical reaction not present on the reversely prepared system. The metal atoms were reported to diffuse into the organic film forming a blurred interface. Moreover, the morphology of organic films acted as substrates for the metal evaporation is inferior to the surface morphology of metallic substrates.

Consequently, the couple of materials forming the contact is an ordered pair since the succession of preparation steps markedly affects the interfacial structure and properties, and both types of interfaces have to be treated separately. Note that the Schottky barrier on traditional semiconductors had been studied via metal evaporation on semiconductor surface, organic semiconductors allow to accomplish both sequences, namely organic-on-metal and metal-on-organic.

##### 4.1 Energy level alignment

If two electronically dissimilar materials make a contact, their distinct energy level positions result in an electronic discontinuity seen by charge carriers as an interfacial electronic barrier. Such interfacial barriers for electrons and holes,  $\varphi_e$  and  $\varphi_h$ , respectively, established between

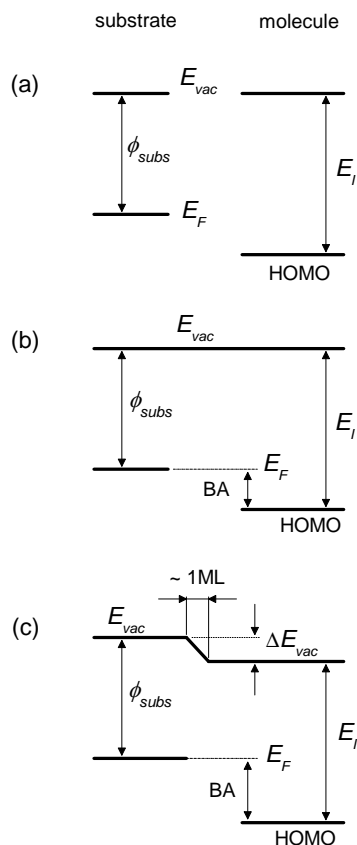


Fig. 4.1. Energy band diagram of a metal-organic pair prior the contact (a), upon the contact with aligned vacuum levels (b), and with vacuum-level offset (c).

the molecular film and metals are shown in Fig. 1.1. The fundamental question is the mechanism governing the alignment of energy levels at the interfaces between the materials forming the contact, and accordingly, the assignment of the initial electronic properties of isolated materials, *i.e.* prior the contact, to the eventual energy level alignment (ELA). The answer would allow the design, control, and prediction of any kind of junction, metal/organic, organic/organic, and semiconductor/organic. As for a metal-organic pair, Figure 4.1a shows energy band diagram of a bare metal and a molecule characterized by  $\phi$  and  $E_I$ , respectively, prior the contact formation. Two fundamental models on the ELA distinguished by (mis)alignment of the vacuum levels have been proposed: (i) the vacuum-level alignment model (Fig. 4.1b) and the interface dipole model (Fig. 4.1c).

The vacuum-level alignment (VLA), which applies for weakly interacting (physisorbed) organic/inorganic systems, had also been referred to the Schottky-Mott rule (or Schottky-Mott limit), inasmuch as the assumption of the VLA was initially employed by Schottky to assess the barrier formed at metal-semiconductor contacts [126, 127]. Provided that the energy levels align

according to the common vacuum level (Fig. 4.1b), the BA is

$$BA = E_I - \phi_{subs}. \quad (4.1)$$

Equation (4.1) implies that the BA is a linear function of the  $\phi_{subs}$  with the slope parameter  $S_{BA} = \Delta BA / \Delta \phi_{subs} = -1$  for each molecular film characterized by its  $E_I$ . The BA insensitive to  $\phi_{subs}$ , *i.e.*,  $S = 0$ , is referred to Bardeen limit. The Schottky-Mott rule had been shown generally unworkable and only part of interfaces (mostly organic heterointerfaces) were reported to obey the VLA.

Disobedience to the VLA model was suggested to be due the vacuum-level offset by amount of  $\Delta E_{vac}$  [Eq. (3.2)], corresponding to a dipole formed at the organic/metal interface, the interfacial dipole (ID) [119] (Fig. 4.1c). The ID controls the barrier across the interface and it is saturated typically upon the completion of the first monolayer. Considering Fig. 4.1c, the relation between the relevant parameters can be written as follows:

$$BA = E_I + ID - \phi_{subs} \quad (4.2)$$

Since the initial parameters  $E_I$  and  $\phi_{subs}$  are known, the knowledge on the mechanism of the ID formation would be essential for the determination of the BA. The dipole model had thereafter attracted a lot of attention and since it has been the most frequently used framework for the description of electronic interfacial properties [27, 93, 128-136]. Various origins of the interfacial charge redistribution were suggested, such as

- (i) The charge redistribution across the interface due to the interaction between a molecule with the substrate surface and eventually chemical bonds formed at the reactive interface [74, 98, 119, 128, 129, 137];
- (ii) Push-back (or pillow) effect [129] meaning that  $\phi_{subs}$  is modified by pushing-back of the tail of the electronic cloud of metal surface by repulsion with the electron cloud of an adsorbate;
- (iii) The interfacial dipole is of quantum origin due to the exchangelike mechanism, not sensitive to electrostatic repulsion or interfacial chemistry [138, 139];
- (iv) Weak chemical reaction between metal and a molecule results in interface states in the organics' gap describable by charge neutrality level, which aligns to the metal Fermi level [130, 140, 141];
- (v) The permanent dipole moment of the adsorbed molecule, the dipole component along the interface normal will induce a potential drop across the interface [131, 136];
- (vi) Charge transfer due to the alignment of the substrate Fermi level and the positive polaronic level of the polymer [142, 143];
- (vii) The equalization of electron chemical potentials of components, *i.e.* the metal work function and  $E_I$  or  $E_{EA}$  of the molecular film [144, 145].

There have been basically two approaches in an experimental search for pivotal parameters of contacting materials determining the ELA: namely, the growth of a particular molecular film on a variety of substrates and the growth of variety molecular films on a particular substrate. In particular, searches for correlations between the metal work function and the  $E_I$  (HOMO) or  $E_{EA}$  (LUMO) have been frequently pursued. For example, no ID– $E_I$  correlation was found for various molecular films grown on gold foil, yet an apparent correlation was observed between the ID and the product  $E_I - 1/2E_t$  [116], where  $E_t$  states for the transport gap. In fact, the observed correlation suggested that the ID is determined—as far as the adsorbed molecule contribution is concerned—by the LUMO position of the molecular film referenced to the vacuum level. This was explicitly claimed in Refs. [20, 76], where the linear correlation between the ID and  $E_{EA}$  for four various phthalocyanines, namely H<sub>2</sub>Pc, CuPc, F<sub>4</sub>CuPc, and F<sub>16</sub>CuPc, and PTCDA, has been observed. Yan *et al.* [146] reported the linear relations between the ID and the product [ $\phi_{subs} - (E_I - E_G/2)$ ]. Such correlation would indicate that the ID is correlated with the *difference* between  $\phi_{subs}$  and the LUMO of the organic film, *i.e.* with the barrier to electron injection from the metal to the organic.

Several studies reported the linear dependences of the ID on the substrate work function [119, 129, 147-152]. However, the claimed linear correlations for specific molecule were typically based on up to three measured values only, with various slope parameters,  $S_{ID} = \Delta E_{vac}/\Delta\phi$ , ranging from 0 to 1 depending on the molecular film. Furthermore, some molecules were reported to reveal two distinct linear dependences; for example, PEN showed the slope parameter either zero or of +1, if grown on substrates with their work function smaller or higher than  $E_I$  of PEN, respectively [153], while quite reverse behaviour has been observed for BCP, *i.e.*, the slope parameters of +1 and zero for small and high substrate work function, respectively [150]. In contrast, no correlation between the ID and the substrate work function has been detected when growing 6T on eight various substrates with work function ranging from about 2 to 5 eV [134].

In terms of the permanent dipole model [131], substrate work function should not show a change upon the growth of a molecule with no permanent dipole, such as *e.g.*, CuPc. Yet, different  $\Delta E_{vac}$ 's were reported for CuPc grown on various substrates with the work function ranging over 1 eV (Tab. 3.2a); the examples rather suggest that  $\Delta E_{vac}$  corresponds to the difference between the substrate work function and the CuPc intrinsic work function of ca 4.4 eV (corresponding to upright-oriented molecules).

#### 4.1.1 Equalization of electrochemical potentials

The work function of a molecular film  $\phi_{film}$  converges to  $\phi_{int}$  with the film thickness (Section 3.2). Accordingly, the total vacuum level change upon the film growth equals to:

$$\Delta E_{vac} = \phi_{subs} - \phi_{int}. \quad (4.3)$$

It is reasonable to presume that the same mechanism for the ELA is valid universally for all film thicknesses (including the monolayer) and Eq. (4.3) then becomes:

$$\Delta E_{vac}(t) = \phi_{subs} - \phi_{film}(t), \quad (4.4)$$

where  $\phi_{film}(t)$  is the function of the thickness  $t$  and  $\phi_{film}$  converges to  $\phi_{int}$  for thickness higher than the critical thickness.

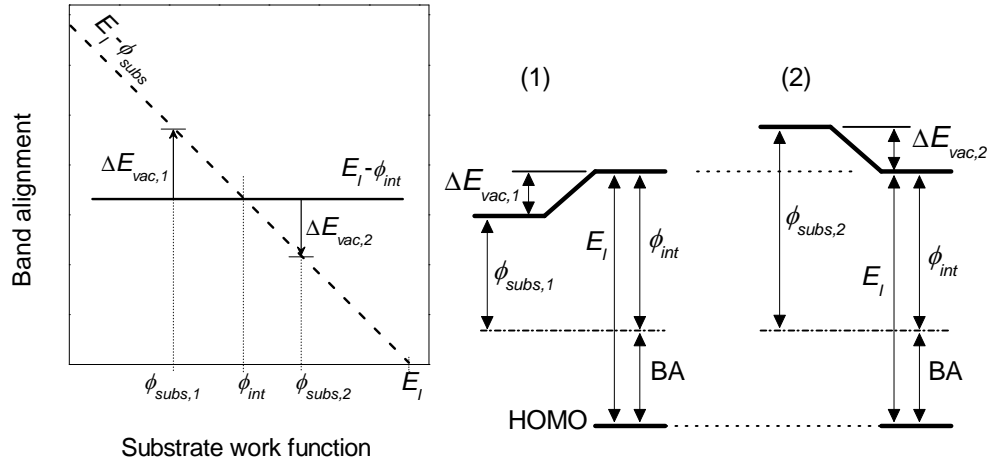


Fig. 4.2. The graphical representation of the BA versus subs in the framework of the model proposing the electrochemical potentials equalization. The solid horizontal line expresses  $BA = E_I - \phi_{int}$ , i.e. the BA insensitive to the substrate work function, the dashed line indicates the Schottky-Mott rule. They intersect at  $\phi_{subs} = \phi_{int}$ . The arrows refer to particular vacuum level changes,  $\Delta E_{vac,1}$  and  $\Delta E_{vac,2}$ , upon the growth onto two substrates with different work functions,  $\phi_{subs,1}$  and  $\phi_{subs,2}$ . Their corresponding band diagrams of the interfaces are sketched at right. Reprinted with permission from J. Ivanco, *Thin Solid Films* **520** (2012) 3975. Copyright 2012, *Elsevier*.

We want to stress that even though Eq. (4.4) is formally identical to Eq. (3.2) employed for the  $\Delta E_{vac}$  determination, Eq. (4.4) expresses the driving force for the vacuum level change: it implies that the Fermi levels of contacting materials defined via their respective (intrinsic) work function, i.e. electrochemical potential of electrons ( $\mu$ ), equalize, whilst the difference between their work functions is compensated by the vacuum level offset. Note that the absolute value of the molecular film's work function matters instead of the work function change.

Knowing the rule for the  $\Delta E_{vac}$  determination [Eq. (4.4)], the BA of a *thick* film determined by photoemission is:

$$BA = E_I - \phi_{int} \quad (4.5)$$

Figure 4.2 presents a graphical representation of Eq. (4.5) for a particular molecular film characterized by the  $E_I$  and grown on various substrates: the BA is independent of the substrate work function as shown by the straight solid line. The arrows (both their length and direction) indicate total vacuum-level changes upon the growth of a thick film onto two distinct substrates with  $\phi_{subs,1}$  and  $\phi_{subs,2}$ . The vacuum-level changes  $\Delta E_{vac,i}$  indicate actually the departure of the  $\mu$ -equalization model from the VLA model, the latter being drawn by a dashed line with the slope of -1. The  $\mu$ -equalization model gives the same result as the VLA model at the intersection of both dependences: the growth of a molecular film with  $\phi_{int}$  onto a substrate with  $\phi_{subs} = \phi_{int}$  results in zero  $\Delta E_{vac}$  upon the contact formation, thereby suggesting the VLA.

The band alignments both independent ( $S = dBA/d\phi_{subs} = 0$ ), i.e. governed by Eq. (4.5) and dependent ( $-0.8 < S < 0$ ) on  $\phi_{subs}$  were reported [56, 129]. In the latter case, we presume—

forasmuch the reported experimental data often lack details such as the film morphology—that the disobedience to Eq. (4.5) may be due to the insufficient film thickness (either nominally or due to the heavy islanding). In such situation, the substrate work function may still affect the measured work function of the film.

Upon the film growth, both signs of the vacuum level change can occur. The downward change occurs provided that molecular films with low  $\phi_{int}$ , such as 6P, 6T, phthalocyanines, or  $\alpha$ -NPD are grown on substrates with high  $\phi$ , either inorganic (*e.g.*, Au, Ni, Pt) or organic (*e.g.*, F<sub>16</sub>CuPc, F<sub>4</sub>TCNQ, PTCDA) ones. In contrast, the upward shift of the vacuum level can be observed provided that molecular films with high  $\phi_{int}$ , such as F<sub>16</sub>CuPc, F<sub>4</sub>TCNQ, PTCDA, or HAT-CN, are grown on substrates with low and moderate work function, either inorganic (*e.g.* Ag, Al, Mg) or organic (*e.g.* CuPc, Alq<sub>3</sub>) ones. Notable, the downward shift of  $E_{vac}$  can change upwardly upon the doping of the low- $\phi_{int}$  film by the high- $\phi_{int}$  molecular film, such as the doping of  $\alpha$ -NPD grown on Au by F<sub>4</sub>TCNQ [56], or by choosing the low- $\phi_{int}$   $\rightarrow$  high- $\phi_{int}$  growth sequence in the organic heterostructure [90]. The vastly frequent reports on downward changes of the vacuum level upon the film growth are obviously owing to the higher popularity of high- $\phi$  substrates employed for the surface studies in combination with frequent molecular films having the moderate or low  $\phi_{int}$ . The infrequent reports on upwards work-function changes had been due to relatively less investigated high- $\phi_{int}$  molecular films, *e.g.* perfluorinated (fluorine substituted) ones, PTCDA, NTCDA, or HAT-CN, grown on substrates with low(er) work function.

Among the listed molecules (Tabs. 3.1 and 3.2), the F<sub>4</sub>TCNQ and HAT-CN have the highest  $\phi_{int}$  of  $\approx 6.25$  eV [154] and  $\approx 6$  eV [89]. The  $\phi_{int}$  magnitudes rank to the highest work functions among the both elements and organics, or Mo-, Cr-, V-, and W-oxides ( $\phi \approx 7$  eV, [145]). The very high  $\phi_{int}$  of F<sub>4</sub>TCNQ and HAT-CN suggests that the film would increase the work function of typical high- $\phi$  elemental surfaces too, such as Au; indeed, the work function of the Au substrate being beyond about 5 eV increased by 0.29 eV upon the growth of even ultrathin film of F<sub>4</sub>TCNQ [155], The trend was confirmed in [156]. Similarly, HAT-CN grown on Au resulted in  $\phi \approx 6.1$  eV [90]. Notable, such molecular film-induced metal work function *increase* would disprove the push-back model [129], which accounts a lowering of the metal work function owing to the compression of the electron tail of metal substrate electrons by the electrons localized in the molecules.

At organic-organic interfaces, no changes of the vacuum level have been presumed due to the charge confinement over a molecule. This indeed applies for heterointerfaces such as ZnPc/CBP, ZnPc/BCP,  $\alpha$ -NPD/BCP,  $\alpha$ -NPD/CBP [157], and PEN/CuPc [158], 6T/6P [159], which showed no or negligible  $\Delta E_{vac}$ . Nevertheless, the vacuum-level changes  $\Delta E_{vac} \approx 0.4$ - $0.5$  eV were observed at the heterostructures such as PTCDA/CuPc, PTCDA/Alq<sub>3</sub> [160], PTCBI/BCP [160], C<sub>60</sub>/CuPc [161], NTCDA/Alq<sub>3</sub>, NTCDA/CuPc, NTCDA/BCP [157], and CuPc/CuPcF<sub>16</sub> [65, 87]. Both trends can be explained in the framework of the electrochemical potential-equalization model: the heterointerfaces in the former group are formed by molecular films with the same or similar  $\phi_{int}$ , while the latter set of examples represents interfaces between molecules with distinct  $\phi_{int}$ . Likewise,  $\Delta E_{vac} \approx 0$  would arise provided that  $\phi_{int}$  of organic films equals to  $\phi$  of an inorganic substrate. Indeed, for example, the PEN on the highly oriented pyrolytic graphite (HOPG) shows the preserved vacuum level; this is apparently due to similar values of  $\phi_{PEN}$  and  $\phi_{HOPG}$  being of  $\sim 4.4$  eV [158].

PPF grown on Ag shown non-monotonous evolution of the  $\Delta E_{vac}$  with the film thickness

[58]: the vacuum level abruptly dropped by 0.42 eV after the first monolayer and remained constant with further growth. Yet,  $E_{vac}$  increased by 0.12 eV at the thickness of 5 nm. The  $F_{16}CuPc$  grown on Au showed a similar non-monotonous evolution [116]. Such curious behaviours of the work function can occur in the perfluorinated molecular film (*i.e.* distinguished by the inequality  $\phi_{int,L} < \phi_{int,U}$ ) provided that the L $\rightarrow$ U orientational transition takes place, and the inequality  $\phi_{int,L} < \phi_{subs} < \phi_{int,U}$  holds. The reversed work function evolution, *i.e.* the work function increase followed by the work function decrease upon the film growth, may occur for an unsubstituted molecular film provided that the inequality  $\phi_{int,L} > \phi_{subs} > \phi_{int,U}$  holds. Indeed, such behaviour of the work function was reported for the growth of titanyl phthalocyanine film on HOPG [162].

The charge neutrality level (CNL) model [130, 132] by Vazquez *et al.* introduces the CNL, the parameter being an intrinsic property of a molecule. The ELA at the molecule/metal interface is determined by the alignment of CNL with the Fermi level of a metal substrate. The calculated CNLs for several molecules are given in Tab. 4.1. The values are similar to  $\phi_{int}$ 's (refer to the next column), which suggests the common origin of both quantities. Admittedly, the comparison is rather preliminary as (*i*) the calculations were based on the one molecule positioned near the substrate surface suggesting that  $\phi_{int}$  was not yet attained, and (*ii*) the statistically meagre ensemble of experimental data on  $\phi_{int}$ 's.

The presented data and proposed ELA mechanism via the equalization of the Fermi levels (see also Ref. [163]) supports the previously reported concepts suggesting that the driving force for the ELA is an equalization of electron chemical potential of metal (corresponding to the metal work function) to that of molecular film [144, 145]; yet, both approaches related the electrochemical potential of the molecular film with its  $E_I$  and  $E_{EA}$  (referred to vacuum level). In this work, the electrochemical potential of a molecular film is—according to the definition and thereby preferable—identified with the intrinsic work function, which is experimentally accessible. The  $\phi_{int}-E_I$  correlation claimed above (Fig. 3.7) would suggest that both parameters are equivalent as far as they change in parallel. Yet, this does not hold for doped semiconductor, where the doping affects the Fermi level and thereby the electrochemical potential, but has no effect on  $E_I$  and  $E_{EA}$ .

Tab. 4.1. The charge-neutrality levels of several molecules [132, 133] and their intrinsic work functions,  $\phi_{int}$ , adopted from Tab. 3.2. Both quantities are referred to the vacuum level.

Molecule	CNL [132] (eV)	CNL [133] (eV)	$\phi_{int}$ [this work] (eV)	
			lying	upright
$\alpha$ -NPD	4.2	-	-	3.8-4.2
Alq <sub>3</sub>	3.8	-	-	$\sim$ 4.0
BCP	3.8	-	-	$\sim$ 4.15
CBP	4.2	4.05	-	$\sim$ 4.5
CuPc	4.0	3.8	-	$\sim$ 3.95
PTCBI	4.4	4.4	-	4.5-4.6
PTCDA	4.8	4.8	4.5-4.94	-



## 4.2 On equivalency between the interfacial dipole and the vacuum-level offset

The interfacial dipole (ID) formed at the organic/metal interface affects the transport barrier for charge carriers injected across the junction. The current concept considers the equivalency between the ID and the measured vacuum-level offset,  $\Delta E_{vac}$ , [recall Eq. (3.3)] detected upon a film growth [119,164]. The concept can be described as follows: Referring back to the definition of the work function, Eq. (3.1) can be formally rewritten and the work function of a bare metal substrate  $\phi_{subs}$

$$\phi_{subs} = \mu_{subs,bulk} + \phi_{subs,SD} \quad (4.6)$$

is modified upon the film growth to

$$\phi_{subs+film} = \mu_{subs,bulk} + \phi_{subs+film,SD}, \quad (4.7)$$

where the indices *subs* and *film* state for the substrate and the film. It is supposed here that the surface-dipole potential of the bare substrate,  $\phi_{subs,SD}$ , is changed to  $\phi_{subs+film,SD}$  upon the film growth. As a result, the substrate work function change  $\Delta\phi$  amounts to

$$\Delta\phi = \phi_{subs} - \phi_{subs+film} = \phi_{subs,SD} - \phi_{subs+film,SD} \equiv \phi_{ID}, \quad (4.8)$$

where  $\phi_{ID}$  is the interface-dipole potential. Note that the ID is an additional dipole to that assigned to the bare substrate surface. We consider the concept inconsequent whereas it assumes a relation between  $\phi_{ID}$  and the final vacuum level even for a thick film, which has to electronically screen out the substrate and the interface. In the following paragraph, an alternative view is proposed.

The quantity  $\Delta\phi$  is routinely yielded by the external photoemission, which means that the spectrometer detects a photoelectron escaping the probed solid. In comparison to the internal ‘transport electron’ passing across the barrier created at the substrate/film interface, the photoelectron is further affected by the film, thus by its electrochemical potential and the surface dipole. It is thereby presumed here that—in variance with the notion expressed by Eq. (4.7)—the work function of the substrate upon the film growth is instead described as follows:

$$\begin{aligned} \phi_{subs+film}^* &= (\mu_{subs,bulk} + \phi_{subs+film,SD})f(1 \xrightarrow{t \rightarrow \infty} 0) \\ &+ (\mu_{film,bulk} + \phi_{film,SD}) \left[ 1 - f(1 \xrightarrow{t \rightarrow \infty} 0) \right], \end{aligned} \quad (4.9)$$

where  $t$  states for the film thickness and  $f(1 \xrightarrow{t \rightarrow \infty} 0)$  is an attenuation function with output converging from unity to zero with the film thickness ranging from near zero to high thickness. The first and second term on the right side of Eq. (4.9) correspond to the substrate and the film, respectively, while  $\phi_{subs+film,SD}$  states for the dipole potential of the substrate surface upon the film formation, thereby the interfacial dipole. Obviously, the work function change  $\Delta\phi = \phi_{subs} - \phi_{subs+film}^*$  obtained by subtracting Eq. (4.6) and Eq. (4.9) is not equal to  $\Delta\phi = \phi_{subs} - \phi_{subs+film}$  [Eq. (4.8)] for the nonzero film term. Admittedly, the first term in Eq. (4.9) can dominate for ultrathin films, *e.g.* one-monolayer thick, yet, it has to converge to zero for thicker overlayers ( $t \rightarrow \infty$ ), where both the substrate and the film/substrate interface are electronically shielded by the film. For a thick film, the second term in Eq. (4.9), which

represents the electrochemical potential of the bulk film and the film surface dipole, dominates and the measured work function is independent of both the substrate and the film/substrate interface. Consequently, the  $\Delta\phi_{subs}$  (or  $\Delta E_{vac}$ ) measured by photoemission upon the film growth converges to the difference between the intrinsic work functions of the substrate and film with the increasing film thickness.

### 4.3 Metal-on-organic interface

The metal growth on organic films may occur in distinct fashions depending on the nature of both the metal and the organic film; the evaporated metals were observed to form chemically reacted [113, 165-176] or inert [172, 177-179] interfaces with the film, to form clusters [167, 180-182] floating on the organic film surface, or the evaporated metal species were reported to diffuse into the bulk of the film [88, 166, 168-174, 183-185].

Compared to the organic-on-metal contacts, the metal-on-organic ones have been mostly focused to examinations of their chemical structure. Understanding the chemical reactions at the interface is a prerequisite for the interface barrier control and some contradicting results on the metal-on-organic systems point to its intricacy. For example, inert metals were reported to form abrupt interface in contrast to the reactive ones diffusing into the organics [172], while the opposite trend was observed in Ref. [168], namely, the in-diffusion of weakly interacting and formation of reacted interface on the organics' surface.

The photoemission studies at the onset of the interface formation obviously deal with minute amounts of metals in the range of—nominally—monolayers. The conclusions on the in-diffusion were often based on the observation that the photoemission signal of an evaporated element was incommensurate to the amount expected on the surface; specifically, the lower photoemission signal indicated a lesser amount of the evaporated metal and thereby suggesting its losses due to diffusion into a bulk, thus out of the probed depth. The chemical reactions are deduced via the 'chemical shift' directly observed by photoemission, that is the (often high- $E_B$ ) shift of a core level corresponding to the reacted element.

The next example illustrates how spurious conclusions, namely a metal diffusion into the organic layer with a concomitant chemical reaction, can be deduced [166]. Figure 4.3 shows the evolution of In  $4d$  core level upon the incremental evaporation of indium onto CuPc film measured at two photon energies of 68 eV (a) and 335 eV (b) to set the 'surface sensitive mode' and 'bulk mode', as the corresponding electron inelastic mean free paths  $\lambda$  were about 2 and 4 monolayers, respectively. A doublet emerging at about 19 eV (Fig. 4.3a), thus shifted by about 2 eV towards high  $E_B$  from the In  $4d$  detected for higher In coverage reveals a reacted component suggesting the reaction between In and CuPc. Yet, the comparison with the measurement at higher photon energy (Fig. 4.3b) suggests that the 'reacted' component is more pronounced in the surface-sensitive mode, it therefore comes out rather from the In surface instead of the In/CuPc interface.

Furthermore, an inspection of the CuPc valence band near the Fermi level (Fig. 4.4) reveals peaks emerging between the HOMO and the Fermi level. The peaks can be interpreted as gap states created in the energy gap of CuPc owing to the reaction between In and CuPc and thereby support the notion on the reactive In/CuPc interface [166].

Yet, photoemission spectra of nanoclusters such as Au and Ag (note that nanoclustering of In on CuPc was confirmed by the secondary electron microscopy [186]) manifest the increasing

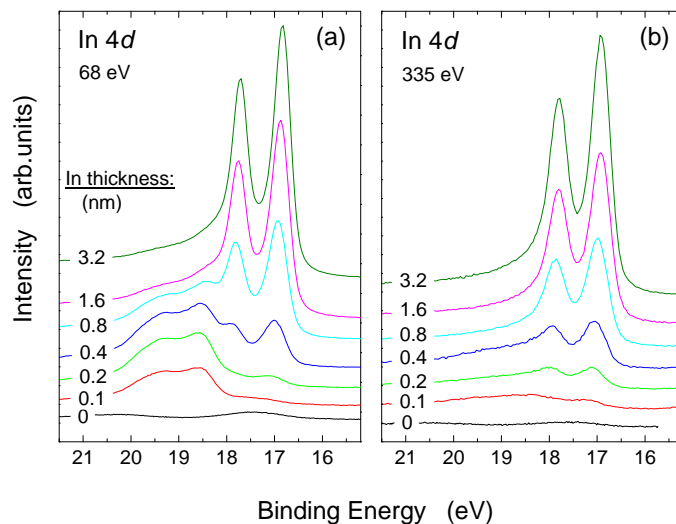


Fig. 4.3. Evolution of the In 4d core-level photoemission spectrum recorded at the photon energy of (a) 68 eV and (b) 335 eV upon the incrementally increased indium deposited on a thick CuPc layer. The nominal indium thicknesses are indicated next to the spectra. Reprinted with permission from J. Ivanco *et al.*, Phys. Rev. B **81** (2010) 115325. Copyright 2010, American Physical Society.

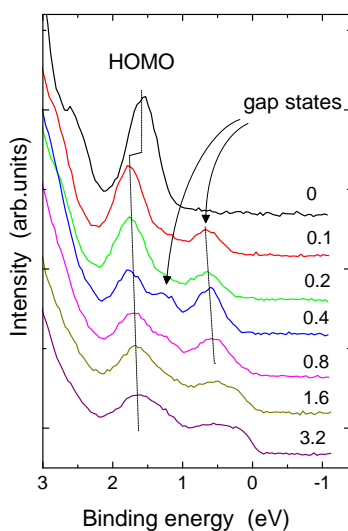


Fig. 4.4. Evolution of the valence band photoemission spectrum of a thick CuPc layer upon the stepwise increased indium coverage. The nominal indium thicknesses in nanometers are given next to the spectra. The arrows indicate new orbitals regarded as gap states. Reprinted with permission from J. Ivanco *et al.*, Phys. Rev. B **81** (2010) 115325. Copyright 2010, American Physical Society.

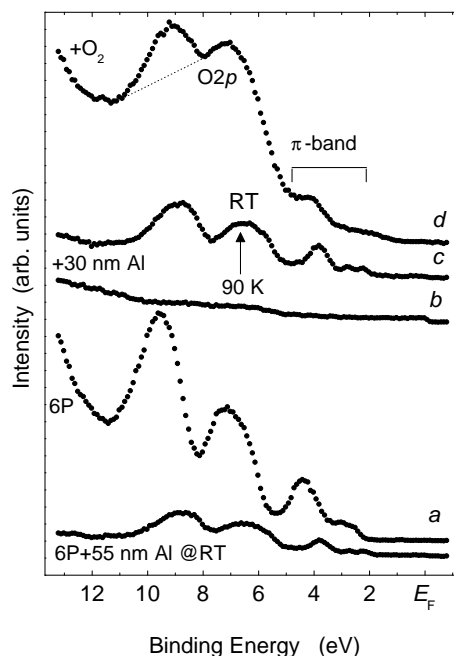


Fig. 4.5. Photoemission spectra of a sexiphenyl film upon 55-nm thick RT-evaporated Al (bottom spectrum). Further spectra: (a) 15 nm sexiphenyl, (b) after adding 30 nm of Al at 90 K, (c) after warming to RT, and (d) after oxygen exposure of 4000 langmuirs. Reprinted with permission from J. Ivanco *et al.*, Appl. Phys. Lett. **85** (2004) 585. Copyright 2004, AIP Publishing LLC.

high- $E_B$  shift with the decreasing size due to the final-state effect [187-192]. Further, the Fermi level edge of such nanoclusters is not developed and the photoemission signal is high- $E_B$  shifted too. Consequently, an ensemble of even inert nanoclusters with varying size can produce superposed spectra with varying shift masquerading as the chemical shift and accordingly to allure a conclusion on the chemical reaction between metal and the substrate. Likewise the core levels, the Fermi edge of nanoclusters is high- $E_B$  shifted and simply superposed to the  $\pi$  band of the underlying molecular film. Accordingly, the mere presence of a feature in the energy band does not prove a chemical reaction. Evidently, not all organic/metal systems are inert; for example, the chemical reaction can occur between metal with a high oxidation potential and molecule comprising oxygen [172].

The In/CuPc system addressed above was prepared in UHV with the base pressure about  $10^{-10}$  mbar. Likewise, aluminium evaporated over sexiphenyl surface in UHV showed marked departure from the laminar growth as the 6P spectra were visible even after nominally 55 nm-thick Al overlayer (bottom spectrum in Fig. 4.5). In contrast, evaporation of nominally only 3 nm-thick Al layer, but at about liquid nitrogen temperature (curve b), led to the complete elimination of the substrate signal of 6P suggesting the laminar growth of Al. Eventually, the 6P spectrum emerged upon warming the Al/6P system to RT (curve c) suggesting either clustering or in-diffusion of Al species. Yet, an oxygen-related feature emerges upon the followed exposure

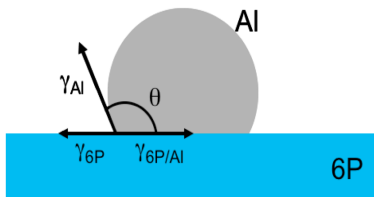


Fig. 4.6. Aluminium island on a surface of sexiphenyl.

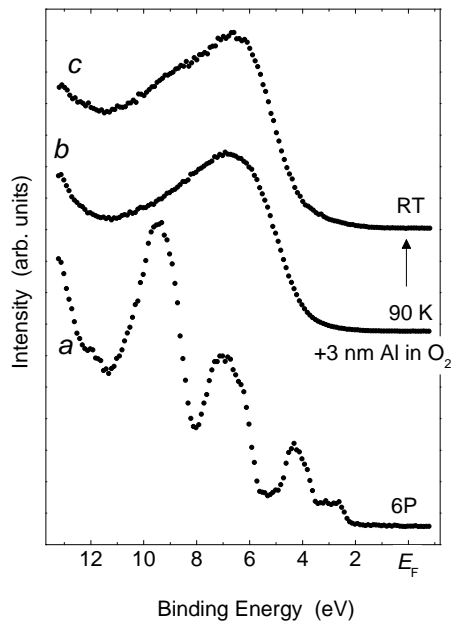


Fig. 4.7. Photoemission spectrum (a) of 15 nm of sexiphenyl, (b) after adding 3 nm of Al evaporated at oxygen pressure of  $10^{-7}$  mbar at 90 K, and (c) upon warming to RT. Reprinted with permission from J. Ivanco *et al.*, Appl. Phys. Lett. **85** (2004) 585. Copyright 2004, AIP Publishing LLC.

to oxygen (curve *d*) implying that aluminium remained on the 6P surface as opposed to the indiffusion.

The clustering of Al on 6P surface (or *e.g.* of In on CuPc discussed above) can be rationalized by means of surface-free energy arguments (Fig. 4.6). The minimization of the total surface free energy of the Al/6P system can be expressed by Young's equation [193]:

$$\gamma_{6P} = \gamma_{Al} \cos \theta + \gamma_{Al/6P}, \quad (4.10)$$

where  $\gamma_{6P}$  and  $\gamma_{Al}$  are the surface free energies of the sexiphenyl substrate and of the Al overlayer, respectively. The  $\gamma_{Al/6P}$  is the interface free energy, and  $\theta$  is the contact angle of the Al island. With  $\gamma_{Al} = 1.1 \text{ Jm}^{-2}$ ,  $\gamma_{6P} \approx 0.03 \text{ Jm}^{-2}$  [194], and  $\gamma_{6P/Al} \sim 0.17 \text{ Jm}^{-2}$  [180], Eq. (4.10) leads to the contact angle  $\theta$  of 97 degree.

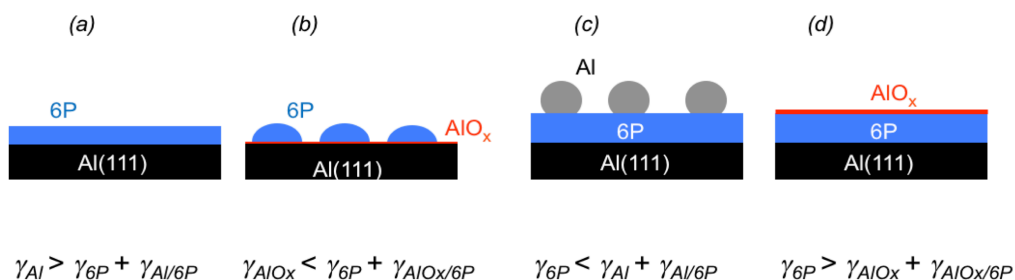


Fig. 4.8. Various process sequences for the preparation of an interface between materials with distinct free surface energies  $\gamma$ , such as Al,  $AlO_x$ , and 6P, whereas  $\gamma_{Al} > \gamma_{AlO_x} \approx \gamma_{6P}$ .

Formation of 3D aluminium clusters naturally imposes a heavy departure from the laminar growth manifested by the markedly delayed onset of Al-related photoemission features; it accordingly leads to the underestimate of the amount of metal located on the surface (bottom curve in Fig. 4.5), and—more importantly—it avoids the formation of continuous 6P/Al interface. The high  $\gamma$  of aluminium, which precludes the wetting of the low- $\gamma$  6P surface, can be diminished by oxidation of Al, since oxidation lowers  $\gamma$ . This is shown in Fig. 4.7, where only 3 nm of Al, however evaporated in high vacuum (with the oxygen partial pressure  $10^{-7}$  mbar) ensures a continuous wetting layer eliminating the signal of underlying 6P film also at RT [180].

Various process sequences examined in Figs. 4.5 and 4.7 are summarized in Fig. 4.8. Due to the inequality  $\gamma_{Al} \gg \gamma_{6P}$ , 3D Al islands are favoured to grow on sexiphenyl surface [Fig. 4.8(c)], and, conversely, sexiphenyl wets the Al surface (panel *a*). If Al is oxidized (*e.g.*, by evaporation in the ambient with higher oxygen partial pressure, such as in high vacuum), the decrease in aluminium surface free energy can reverse the inequality and result in wetting of the sexiphenyl surface (panel *d*). For sexiphenyl tends to grow on  $AlO_x$  in Stransky-Krastanov or Volmer-Weber growth fashion, apparently  $\gamma_{6P}$  approximately equals or is higher than  $\gamma_{AlO_x}$  (panel *b*).

## 5 Summary

The review addresses electronic, chemical, and geometric properties of electronically active molecular film and related interfaces probed by photoemission, which are pursued with the consideration to the molecular orientation. It accents several issues necessary to consider while employing photoemission characterization for examination of molecular films and related interfaces. In essence:

- Dependence of electronic properties on the molecular orientation necessitates the extension of the standard discernment of growth fashions (laminar, islanding). Neglecting to consider the molecular orientation can lead to erroneous conclusions on the presence of band bending as the effect of varying work function implied by the orientational transition of molecules masquerades as the band bending.
- Molecular films can be characterized by their intrinsic work function analogously to inorganic elemental electronic materials (*e.g.* metals). The intrinsic work function of molecular films is an experimentally accessible and it is an essential parameter in reference to the proposed model on energy level alignment (ELA); the model accounts the equalization of electrochemical potentials of materials forming a contact to be the controlling mechanism for the ELA at the film/substrate interface.
- The vacuum-level offset  $\Delta E_{vac}$  measured by photoemission upon the film growth converges to the difference between the initial work functions of the substrate and the intrinsic work function of the film with the increasing film thickness.
- Interaction-strength model employed to rationalize the lying and upright molecular orientation seems invalid and the molecular orientation of rod-like molecules is determined by the morphology of the substrate surface.
- Due to markedly higher surface free energy of metal compared to organic, metal does not wet the organics' surface in the absence of chemical reaction and the formation of 3D metal nanoclusters are favoured at onset of the interface formation. Neglecting the metal morphology on photoemission characterization in this stage can eventuate in erroneous conclusions on the interfacial chemical and electronic structure.

### Acknowledgement

The supports of the Slovak Research and Development Agency under project No. APVV-0096-11 and from Grant Agency VEGA Bratislava under project No.2/0162/12 are acknowledged.

## References

- [1] R. McNeill, R. Siudak, J. Wardlaw, D. Weiss, *Austr. J. Chem.* **16** (1963) 1056.
- [2] B. Bolto, D. Weiss, *Austr. J. Chem.* **16** (1963) 1076.
- [3] C.W. Tang, A.C. Albrecht, *J. Chem. Phys.* **62** (1975) 2139.
- [4] C.K. Chiang, C.R. Fincher, Y.W. Park, A.J. Heeger, H. Shirakawa, E.J. Louis, S.C. Gau, A.G. MacDiarmid, *Phys. Rev. Lett.* **39** (1977) 1098.
- [5] C.K. Chiang, C.R. Fincher, Y.W. Park, A.J. Heeger, H. Shirakawa, E.J. Louis, S.C. Gau, A.G. MacDiarmid, *Phys. Rev. Lett.* **40** (1978) 1472.
- [6] G.A. Chamberlain, *Solar Cells* **10** (1983) 199.
- [7] G.A. Chamberlain, *Solar Cells* **8** (1983) 47.
- [8] C.W. Tang, *Appl. Phys. Lett.* **48** (1986) 183.
- [9] C.W. Tang, S.A. VanSlyke, *Appl. Phys. Lett.* **51** (1987) 913.
- [10] G. Horowitz, D. Fichou, X. Peng, Z. Xu, F. Garnier, *Solid State Commun.* **72** (1989) 381.
- [11] B. Servet, G. Horowitz, S. Ries, O. Lagorsse, P. Alnot, A. Yassar, F. Deloffre, P. Srivastava, R. Hajlaoui, P. Lang, F. Garnier, *Chem. Mater.* **6** (1994) 1809.
- [12] J.H. Burroughes, D.D.C. Bradley, A.R. Brown, R.N. Marks, K. Mackay, R.H. Friend, P.L. Burns, A.B. Holmes, *Nature* **347** (1990) 539.
- [13] R.N. Marks, J.J. M Halls, D.D.C. Bradley, R.H. Friend, A.B. Holmes, *J. Phys. C: Condens. Matter* **6** (1994) 1379.
- [14] G. Yu, J. Gao, J.C. Hummelen, F. Wudl, A.J. Heeger, *Science* **270** (1995) 1789.
- [15] F. Garnier, R. Hajlaoui, A. Yassar, P. Srivastava, *Science* **265** (1994) 1684.
- [16] J.J. Yeh, I. Lindau, *Atomic Data and Nuclear Data Tables* **32** (1985) 1.
- [17] G. Koller, S. Berkebile, J. Ivanco, F.P. Netzer, M.G. Ramsey, *Surf. Sci.* **601** (2007) 5683.
- [18] P. Stadler, A.M. Track, M. Ullah, H. Sitter, G.J. Matt, G. Koller, T.B. Singh, H. Neugebauer, N.S. Saricifci, M.G. Ramsey, *Org. Electron.* **11** (2010) 207.
- [19] T. Toader, G. Gavrilă, W. Braun, J. Ivanco, D.R.T. Zahn, *Phys. Stat. Sol. (b)* **246** (2009) 1510.
- [20] D.R.T. Zahn, G.N. Gavrilă, M. Gorgoi, *Chem. Phys.* **325** (2006) 99.
- [21] S. Krause, M.B. Casu, A. Schöll, E. Umbach, *New J. Phys.* **10** (2008) 085001.
- [22] H. Yanagi, S. Okamoto, *Appl. Phys. Lett.* **71** (1997) 2563.
- [23] B.P. Rand, D. Cheyons, K. Vasseur, N.C. Giebink, S. Mothy, Y. Yi, V. Coropceanu, D. Beljonne, J. Cornil, J.-L. Brédas, J. Genoe, *Adv. Funct. Mater.* **22** (2012) 2987.
- [24] A. Ojala, A. Petersen, A. Fuchs, R. Lovrincic, C. Pölking, J. Trollmann, J. Hwang, C. Lennartz, H. Reichelt, H.W. Höffken, A. Pucci, P. Erk, T. Kirchartz, F. Würthner, *Adv. Funct. Mater.* **22** (2012) 86.
- [25] D. Oelkrug, H.J. Egelhaaf, J. Haiber, *Thin Solid Films* **284–285** (1996) 267.
- [26] P. Lang, M.E. Ardhaoui, J.C. Wittmann, J.P. Dallas, G. Horowitz, B. Lotz, F. Garnier, C. Straupe, *Synth. Met.* **84** (1997) 605.
- [27] J. Ivanco, J.R. Krenn, M.G. Ramsey, F.P. Netzer, T. Haber, R. Resel, A. Haase, B. Stadlober, G. Jakopic, *J. Appl. Phys.* **96** (2004) 2716.
- [28] M.A. Loi, E. Da Como, F. Dinelli, M. Murgia, R. Zamboni, F. Biscarini, M. Muccini, *Nat. Mater.* **4** (2005) 81.
- [29] R. Garcia, M. Tello, J.F. Moulin, F. Biscarini, *Nano Lett.* **4** (2004) 1115.



- [30] S. Prato, L. Floreano, D. Cvetko, V.D. Renzi, A. Morgante, S. Modesti, F. Biscarini, R. Zamboni, C. Taliani, *J. Phys. Chem. B* **103** (1999) 7788.
- [31] G. Yoshikawa, M. Kiguchi, S. Ikeda, K. Saiki, *Surf. Sci.* **559** (2004) 77.
- [32] B. Winter, S. Berkebile, J. Ivanco, G. Koller, F.P. Netzer, M.G. Ramsey, *Appl. Phys. Lett.* **88** (2006) 253111.
- [33] T. Okajima, S. Narioka, S. Tanimura, K. Hamano, T. Kurata, Y. Uehara, T. Araki, H. Ishii, Y. Ouchi, K. Seki, T. Ogama, H. Koezuka, *J. Electron Spectrosc. Rel. Phenom.* **78** (1996) 379.
- [34] H. Peisert, T. Schwieger, J.M. Auerhammer, M. Knupfer, M.S. Golden, J. Fink, P.R. Bressler, M. Mast, *J. Appl. Phys.* **90** (2001) 466.
- [35] M. Oehzelt, R. Resel, C. Suess, R. Friedlein, W.R. Salaneck, *J. Chem. Phys.* **124** (2006) 054711.
- [36] J. Ivanco, T. Haber, J.R. Krenn, F.P. Netzer, R. Resel, M.G. Ramsey, *Surf. Sci.* **601** (2007) 178.
- [37] M. Oehzelt, Leonhard Grill, L.S. Berkebile, G. Koller, F.P. Netzer, M.G. Ramsey, *ChemPhysChem* **8** (2007) 1707.
- [38] M. Koini, T. Haber, S. Berkebile, G. Koller, M.G. Ramsey, R. Resel, M. Oehzelt, *J. Cryst. Growth* **311** (2009) 1364.
- [39] T. Toader, G. Gavrilă, J. Ivanco, W. Braun, D.R.T. Zahn, *Appl. Surf. Sci.* **255** (2009) 6806.
- [40] W.S. Hu, Y.F. Lin, Y.T. Tao, Y.J. Hsu, D.H. Wei, *Macromolecules* **38** (2005) 9617.
- [41] M. Oehzelt, G. Koller, J. Ivanco, S. Berkebile, T. Haber, R. Resel, F.P. Netzer, M.G. Ramsey, *Adv. Mater.* **18** (2006) 2466.
- [42] T. Breuer, I. Salzmänn, J. Gotzen, M. Oehzelt, A. Morherr, N. Koch, G. Witte, *Crystal Growth & Design* **11** (2011) 4996.
- [43] M. Kiguchi, G. Yoshikawa, K. Saiki, *J. Appl. Phys.* **94** (2003) 4866.
- [44] B. Winter, J. Ivanco, F.P. Netzer, M.G. Ramsey, *Thin Solid Films* **433** (2003) 269.
- [45] S. Duhm, H. Glowatzki, J.P. Rabe, N. Koch, R.L. Johnson, *Appl. Phys. Lett.* **88** (2006) 203109.
- [46] S. Kowarik, A. Gerlach, S. Sellner, F. Schreiber, L. Cavalcanti, O. Kononov, *Phys. Rev. Lett.* **96** (2006) 125504.
- [47] H. Peisert, I. Biswas, L. Zhang, M. Knupfer, M. Hanack, D. Dini, M.J. Cook, I. Chambrier, T. Schmidt, D. Batchelor, T. Chassé, *Chem. Phys. Lett.* **403** (2005) 1.
- [48] C.E. Heiner, J. Dreyer, I.V. Hertel, N. Koch, H.H. Ritze, W. Widdra, B. Winter, *Appl. Phys. Lett.* **87** (2005) 093501.
- [49] H. Glowatzki, G.N. Gavrilă, S. Seifert, R.L. Johnson, J. Rader, K. Mullen, D.R.T. Zahn, J.P. Rabe, N. Koch, *J. Phys. Chem. C* **112** (2008) 1570.
- [50] T. Haber, S. Muellegger, A. Winkler, R. Resel, *Phys. Rev. B* **74** (2006) 045419.
- [51] R.J. Kline, M.D. McGehee, M.F. Toney, *Nat. Mater.* **5** (2006) 222.
- [52] M. Cerminara, R. Tubino, F. Meinardi, J. Ivanco, F.P. Netzer, M.G. Ramsey, *Thin Solid Films* **516** (2008) 4247.
- [53] N. Sato, K. Seki, H. Inokuchi, *J. Chem. Soc., Faraday Trans. 2* **77** (1981) 1621.
- [54] W.R. Salaneck, *Phys. Rev. Lett.* **40** (1978) 60.
- [55] C. Falkenberg, S. Olthof, R. Rieger, M. Baumgarten, K. Muellen, K. Leo, M. Riede, *Solar Energy Materials and Solar Cells* **95** (2011) 927.
- [56] A. Kahn, N. Koch, W. Gao, *J. Polym. Sci. B: Polym. Phys.* **41** (2003) 2529.
- [57] J. Meiss, A. Merten, M. Hein, C. Schuenemann, S. Schäfer, M. Tietze, C. Urich, M. Pfeiffer, K. Leo, M. Riede, *Adv. Funct. Mater.* **22** (2012) 405.
- [58] S. Duhm, S. Hosoumi, I. Salzmänn, A. Gerlach, M. Oehzelt, B. Wedl, T.-L. Lee, F. Schreiber, N. Koch, N. Ueno, S. Kera, *Phys. Rev. B* **81** (2010) 045418.

- [59] D.M. Alloway, A.L. Graham, X. Yang, A. Mudalige, R. Colorado, V.H. Wysocki, J.E. Pemberton, T. Randall Lee, R.J. Wysocki, N.R. Armstrong, *J. Phys. Chem. C* **113** (2009) 20328.
- [60] J. Ivanco, B. Winter, F.P. Netzer, M.G. Ramsey, *Adv. Mater.* **15** (2003) 1812.
- [61] R. Telesca, H. Bolink, S. Yunoki, G. Hadziioannou, P.T. Van Duijnen, J.G. Snijders, H.T. Jonkman, G.A. Sawatzky, *Phys. Rev. B* **63** (2001) 155112.
- [62] M.B. Casu, P. Imperia, J.E. Wong, S. Schrader, *Synth. Met.* **138** (2003) 131.
- [63] S. Duhm, G. Heimel, I. Salzmänn, H. Glowatzki, R.L. Johnson, A. Vollmer, J.P. Rabe, N. Koch, *Nat. Mater.* **7** (2008) 326.
- [64] T.S. Ellis, K.T. Park, S.L. Hulbert, M.D. Ulrich, J.E. Rowe, *J. Appl. Phys.* **95** (2004) 982.
- [65] W. Chen, D.C. Qi, Y.L. Huang, H. Huang, Y.Z. Wang, S. Chen, X.Y. Gao, A.T.S. Wee, *J. Phys. Chem. C* **113** (2009) 12832.
- [66] M. Gorgoi, D.R.T. Zahn, *Org. Electron.* **6** (2005) 168.
- [67] H. Fukagawa, H. Yamane, T. Kataoka, S. Kera, M. Nakamura, K. Kudo, N. Ueno, *Phys. Rev. B* **73** (2006) 245310.
- [68] W. Chen, D.-C. Qi, H. Huang, X. Gao, A.T.S. Wee, *Adv. Funct. Mater.* **21** (2011) 410.
- [69] I. Salzmänn, S. Duhm, G. Heimel, M. Oehzelt, R. Kniprath, R.L. Johnson, J. Rabe, P., N. Koch, *J. Am. Chem. Soc.* **130** (2008) 12870.
- [70] N. Koch, A. Vollmer, S. Duhm, Y. Sakamoto, T. Suzuki, *Adv. Mater.* **19** (2007) 112.
- [71] J.W. Keister, J.E. Rowe, J.J. Kolodziej, T.E. Madey, *J. Vac. Sci. Technol. A* **18** (2000) 2174.
- [72] H. Hornauer, J. Vancea, G. Reiss, H. Hoffmann, *Z. Phys. B - Condens. Mat.* **77** (1989) 399.
- [73] F. Petraki, V. Papaefthimiou, S. Kennou, *Org. Electron.* **8** (2007) 522.
- [74] I.G. Hill, J. Schwartz, A. Kahn, *Org. Electron.* **1** (2000) 5.
- [75] Y. Ge, J.E. Whitten, *J. Phys. Chem. C* **112** (2008) 1174.
- [76] S. Park, T.U. Kampen, D.R.T. Zahn, W. Braun, *Appl. Phys. Lett.* **79** (2001) 4124.
- [77] N.J. Watkins, Y. Gao, *J. Appl. Phys.* **94** (2003) 1289.
- [78] N. Koch, A. Gerlach, S. Duhm, H. Glowatzki, G. Heimel, A. Vollmer, Y. Sakamoto, T. Suzuki, J. Zegenhagen, J.P. Rabe, F. Schreiber, *J. Am. Chem. Soc.* **130** (2008) 7300.
- [79] M. Grobosch, M. Knupfer, *Adv. Mater.* **19** (2007) 754.
- [80] E.W. Forsythe, V.-E. Choong, T.Q. Le, Y. Gao, *J. Vac. Sci. & Technol. A* **17** (1999) 3429.
- [81] N. Koch, A. Kahn, J. Ghijsen, J.J. Pireaux, J. Schwartz, R.L. Johnson, A. Elschner, *Appl. Phys. Lett.* **82** (2003) 70.
- [82] W. Gao, A. Kahn, *Appl. Phys. Lett.* **82** (2003) 4815.
- [83] Y. Gao, H. Ding, H. Wang, D. Yan, *Appl. Phys. Lett.* **91** (2007) 142112.
- [84] M. Knupfer, H. Peisert, *Phys. Stat. Sol. (a)* **201** (2004) 1055.
- [85] H. Peisert, M. Knupfer, *J. Fink, Surf. Sci.* **515** (2002) 491.
- [86] H. Peisert, M. Knupfer, T. Schwieger, J.M. Auerhammer, M.S. Golden, J. Fink, *J. Appl. Phys.* **91** (2002) 4872.
- [87] K.M. Lau, J.X. Tang, H.Y. Sun, C.S. Lee, S.T. Lee, D. Yan, *Appl. Phys. Lett.* **88** (2006) 173513.
- [88] C. Shen, A. Kahn, *J. Appl. Phys.* **90** (2001) 4549.
- [89] H. Kang, J.-H. Kim, J.-K. Kim, J. Seo, Y. Park, *J. Korean Phys. Soc.* **59** (2011) 3060.
- [90] Y.-K. Kim, J. Won Kim, Y. Park, *Appl. Phys. Lett.* **94** (2009) 063305.
- [91] N.J. Watkins, Y. Gao, *J. Appl. Phys.* **94** (2003) 5782.
- [92] I. Salzmänn, S. Duhm, R. Opitz, R.L. Johnson, J.P. Rabe, N. Koch, *J. Appl. Phys.* **104** (2008) 114518.

- [93] A. Rajagopal, C.I. Wu, A. Kahn, *J. Appl. Phys.* **83** (1998) 2649.
- [94] X. Liu, M. Knupfer, B.H. Huisman, *Surf. Sci.* **595** (2005) 165.
- [95] D.R. Lide, *Handbook of Chemistry and Physics*, CRC Press, Inc., Boca Raton, 1994.
- [96] K. Seki, N. Hayashi, H. Oji, E. Ito, Y. Ouchi, H. Ishii, *Thin Solid Films* **393** (2001) 298.
- [97] S.T. Lee, X.Y. Hou, M.G. Mason, C.W. Tang, *Appl. Phys. Lett.* **72** (1998) 1593.
- [98] G. Paasch, H. Peisert, M. Knupfer, J. Fink, S. Scheinert, *J. Appl. Phys.* **93** (2003) 6084.
- [99] I.G. Hill, A.J. Makinen, Z.H. Kafafi, *Appl. Phys. Lett.* **77** (2000) 1825.
- [100] I. Biswas, H. Peisert, M. Nagel, M.B. Casu, S. Schuppler, P. Nagel, E. Pellegrin, T. Chasse, *J. Chem. Phys.* **126** (2007) 174704.
- [101] H. Yamane, Y. Yabuuchi, H. Fukagawa, S. Kera, K.K. Okudaira, N. Ueno, *J. Appl. Phys.* **99** (2006) 093705.
- [102] J. Ivanco, T. Haber, R. Resel, F.P. Netzer, M.G. Ramsey, *Thin Solid Films* **514** (2006) 156.
- [103] W. Chen, H. Huang, S. Chen, Y.L. Huang, X.Y. Gao, A.T.S. Wee, *Chem. Mater.* **20** (2008) 7017.
- [104] W. Chen, H. Huang, S. Chen, X.Y. Gao, A.T.S. Wee, *J. Phys. Chem. C* **112** (2008) 5036.
- [105] L. Huang, C. Liu, B. Yu, J. Zhang, Y. Geng, D. Yan, *J. Phys. Chem. B* **114** (2010) 4821.
- [106] I. Arbi, B.B. Hamada, A. Souissi, S. Menzli, C.B. Azzouz, A. Laribi, A. Akremi, C. Chefi, *Appl. Surf. Sci.* **305** (2014) 396.
- [107] S.M. Sze, K.N. Kwok, *Physics of Semiconductor Devices*, Wiley-Interscience, New York, 2007.
- [108] R.C. Weast, *CRC Handbook of Chemistry and Physics*, CRC Press, Boca Raton, FL, 1984-1985.
- [109] H. Kobayashi, K. Namba, T. Mori, Y. Nakato, *Phys. Rev. B* **52** (1995) 5781.
- [110] B. Lu, H.J. Zhang, H.Y. Li, S.N. Bao, P. He, T.L. Hao, *Phys. Rev. B* **68** (2003) 125410.
- [111] P.G. Schroeder, C.B. France, B.A. Parkinson, R. Schlaf, *J. Appl. Phys.* **91** (2002) 9095.
- [112] V. Papaefthimiou, A. Siokou, S. Kennou, *J. Appl. Phys.* **91** (2002) 4213.
- [113] J.X. Tang, C.S. Lee, S.T. Lee, *Appl. Surf. Sci.* **252** (2006) 3948.
- [114] H. Ishii, N. Hayashi, E. Ito, Y. Washizu, K. Sugi, Y. Kimura, M. Niwano, Y. Ouchi, K. Seki, *Phys. Stat. Sol. (a)* **201** (2004) 1075.
- [115] T. Nishi, K. Kanai, Y. Ouchi, M.R. Willis, K. Seki, *Chem. Phys. Lett.* **414** (2005) 479.
- [116] H. Peisert, M. Knupfer, J. Fink, *Appl. Phys. Lett.* **81** (2002) 2400.
- [117] G. Ertl, J. Koppers, *Low Energy Electrons and Surface Chemistry*, VCH, Weinheim, 1985.
- [118] J. Ivanco, D.R.T. Zahn, *J. Vac. Sci. Technol. A* **27** (2009) 1178.
- [119] S. Narioka, H. Ishii, D. Yoshimura, M. Sei, Y. Ouchi, K. Seki, S. Hasegawa, T. Miyazaki, Y. Harima, K. Yamashita, *Appl. Phys. Lett.* **67** (1995) 1899.
- [120] G. Koller, B. Winter, M. Oehzelt, J. Ivanco, F.P. Netzer, M.G. Ramsey, *Org. Electron.* **8** (2007) 63.
- [121] F. Evangelista, V. Carravetta, G. Stefani, B. Jansik, M. Alagia, S. Stranges, A. Ruocco, *J. Chem. Phys.* **126** (2007) 124709.
- [122] V.Y. Aristov, O.V. Molodtsova, V. Maslyuk, D.V. Vyalikh, V.M. Zhilin, Y.A. Ossipyan, T. Bredow, I. Mertig, M. Knupfer, *Appl. Surf. Sci.* **254** (2007) 20.
- [123] F. Song, H. Huang, W. Dou, H. Zhang, Y. Hu, H. Qian, H. Li, P. He, S. Bao, Q. Chen, W. Zhou, *J. Phys.: Condens. Matter* **19** (2007) 8.
- [124] M.-S. Liao, S. Scheiner, *J. Chem. Phys.* **114** (2001) 9780.
- [125] L. Lozzi, S. Santucci, S. La Rosa, B. Delley, S. Picozzi, *J. Chem. Phys.* **121** (2004) 1883.
- [126] N.F. Mott, *Proc. R. Soc. London* **171** (1939) 27.
- [127] W. Schottky, *Phys. Z.* **41** (1940) 570.

- [128] I.G. Hill, A. Rajagopal, A. Kahn, Y. Hu, *Appl. Phys. Lett.* **73** (1998) 662.
- [129] H. Ishii, K. Sugiyama, E. Ito, K. Seki, *Adv. Mater.* **11** (1999) 605.
- [130] H. Vázquez, F. Flores, R. Oszwaldowski, J. Ortega, R. Pérez, A. Kahn, *Appl. Surf. Sci.* **234** (2004) 107.
- [131] S. Kera, Y. Yabuuchi, H. Yamane, H. Setoyama, K.K. Okudaira, A. Kahn, N. Ueno, *Phys. Rev. B* **70** (2004) 085304.
- [132] H. Vázquez, W. Gao, F. Flores, A. Kahn, *Phys. Rev. B* **71** (2005) 041306.
- [133] H. Vazquez, Y.J. Dappe, J. Ortega, F. Flores, *J. Chem. Phys.* **126** (2007) 144703.
- [134] J. Ivanco, F.P. Netzer, M.G. Ramsey, *J. Appl. Phys.* **101** (2007) 103712.
- [135] H. Yamane, H. Honda, H. Fukagawa, M. Ohyama, Y. Hinuma, S. Kera, K.K. Okudaira, N. Ueno, *J. Electron Spectrosc. Rel. Phenom.* **137-140** (2004) 223.
- [136] T. Bauert, L. Zoppi, G. Koller, A. Garcia, K.K. Baldrige, K.-H. Ernst, *J. Phys. Chem. Lett.* **2** (2011) 2805.
- [137] H. Ishii, K. Seki, *Electron Devices, IEEE Transactions on* **44** (1997) 1295.
- [138] P.S. Bagus, V. Staemmler, C. Wöll, *Phys. Rev. Lett.* **89** (2002) 096104.
- [139] V. De Renzi, R. Rousseau, D. Marchetto, R. Biagi, S. Scandolo, U. del Pennino, *Phys. Rev. Lett.* **95** (2005) 046804.
- [140] H. Vazquez, R. Oszwaldowski, P. Pou, J. Ortega, R. Perez, F. Flores, A. Kahn, *Europhys. Lett.* **65** (2004) 802.
- [141] H. Vazquez, F. Flores, A. Kahn, *Org. Electron.* **8** (2007) 241.
- [142] C. Tengstedt, W. Osikowicz, W.R. Salaneck, I.D. Parker, C.-H. Hsu, M. Fahlman, *Appl. Phys. Lett.* **88** (2006) 053502.
- [143] S. Braun, W. Salaneck, R. , M. Fahlman, *Adv. Mater.* **21** (2009) 1450.
- [144] X. Crispin, V. Geskin, A. Crispin, J. Cornil, R. Lazzaroni, W.R. Salaneck, J.L. Bredas, *J. Am. Chem. Soc.* **124** (2002) 8131.
- [145] M.T. Greiner, M.G. Helander, W.-M. Tang, Z.-B. Wang, J. Qiu, Z.-H. Lu, *Nat. Mater.* **11** (2012) 76.
- [146] L. Yan, N.J. Watkins, S. Zorba, Y. Gao, C.W. Tang, *Appl. Phys. Lett.* **79** (2001) 4148.
- [147] I.G. Hill, A. Rajagopal, A. Kahn, *J. Appl. Phys.* **84** (1998) 3236.
- [148] N.J. Watkins, L. Yan, Y. Gao, *Appl. Phys. Lett.* **80** (2002) 4384.
- [149] L. Yan, N.J. Watkins, S. Zorba, Y. Gao, C.W. Tang, *Appl. Phys. Lett.* **81** (2002) 2752.
- [150] T. Sakurai, S. Toyoshima, H. Kitazume, S. Masuda, H. Kato, K. Akimoto, *J. Appl. Phys.* **107** (2010) 043707.
- [151] N. Koch, *J. Phys.: Condens. Matter* **20** (2008) 184008.
- [152] S. Braun, W.R. Salaneck, *Chem. Phys. Lett.* **438** (2007) 259.
- [153] H. Fukagawa, S. Kera, T. Kataoka, S. Hosoumi, Y. Watanabe, K. Kudo, N. Ueno, *Adv. Mater.* **19** (2007) 665.
- [154] S. Winkler, J. Frisch, R. Schlesinger, M. Oehzelt, R. Rieger, H.J. Räder, J.P. Rabe, K. Mullen, N. Koch, *J. Phys. Chem. C* **117** (2013) 22285.
- [155] G.M. Rangger, O.T. Hofmann, L. Romaner, G. Heimel, B. Broker, R.-P. Blum, R.L. Johnson, N. Koch, E. Zojer, *Phys. Rev. B* **79** (2009) 165306.
- [156] N. Koch, S. Duhm, J.P. Rabe, A. Vollmer, R.L. Johnson, *Phys. Rev. Lett.* **95** (2005) 237601.
- [157] A. Kahn, W. Zhao, W. Gao, H. Vázquez, F. Flores, *Chem. Phys.* **325** (2006) 129.
- [158] M.L. Blumenfeld, M.P. Steele, O.L.A. Monti, *J. Phys. Chem. Lett.* **1** (2010) 145.

- [159] G. Schwabegger, M. Oehzelt, I. Salzmann, F. Quochi, M. Saba, A. Mura, G. Bongiovanni, A. Vollmer, N. Koch, H. Sitter, C. Simbrunner, *Langmuir* **29** (2013) 14444.
- [160] I.G. Hill, D. Milliron, J. Schwartz, A. Kahn, *Appl. Surf. Sci.* **166** (2000) 354.
- [161] O.V. Molodtsova, T. Schwieger, M. Knupfer, *Appl. Surf. Sci.* **252** (2005) 143.
- [162] H. Fukagawa, H. Yamane, S. Kera, K.K. Okudaira, N. Ueno, *Phys. Rev. B* **73** (2006) 041302.
- [163] J. Ivano, *Thin Solid Films* **520** (2012) 3975.
- [164] R.T. Tung, *Phys. Rev. Lett.* **84** (2000) 6078.
- [165] G. Gavrilu, D.R.T. Zahn, W. Braun, *Appl. Phys. Lett.* **89** (2006) 162102.
- [166] V.Y. Aristov, O.V. Molodtsova, V.M. Zhilin, D.V. Vyalikh, M. Knupfer, *Phys. Rev. B* **72** (2005) 165318.
- [167] H. Ahn, J.E. Whitten, *J. Appl. Phys.* **93** (2003) 3384.
- [168] M. Probst, R. Haight, *Appl. Phys. Lett.* **70** (1997) 1420.
- [169] A. Rajagopal, A. Kahn, *J. Appl. Phys.* **84** (1998) 355.
- [170] V.Y. Aristov, O.V. Molodtsova, Y.A. Ossipyan, B.P. Doyle, S. Nannarone, M. Knupfer, *Org. Electron.* **10** (2009) 8.
- [171] D.R.T. Zahn, G.N. Gavrilu, G. Salvan, *Chem. Rev.* **107** (2007) 1161.
- [172] Y. Hirose, A. Kahn, V. Aristov, P. Soukiasian, V. Bulovic, S.R. Forrest, *Phys. Rev. B* **54** (1996) 13748.
- [173] Y. Tai, A. Shaporenko, W. Eck, M. Grunze, M. Zharnikov, *Appl. Phys. Lett.* **85** (2004) 6257.
- [174] T.U. Kampen, A. Das, S. Park, W. Hoyer, D.R.T. Zahn, *Appl. Surf. Sci.* **234** (2004) 333.
- [175] C. Shen, A. Kahn, J. Schwartz, *J. Appl. Phys.* **89** (2001) 449.
- [176] Q. Toan Le, L. Yan, Y. Gao, M.G. Mason, D.J. Giesen, C.W. Tang, *J. Appl. Phys.* **87** (2000) 375.
- [177] M. Gorgoi, D.R.T. Zahn, *Appl. Surf. Sci.* **252** (2006) 5453.
- [178] O.V. Molodtsova, V.Y. Aristov, V.M. Zhilin, Y.A. Ossipyan, D.V. Vyalikh, B.P. Doyle, S. Nannarone, M. Knupfer, *Appl. Surf. Sci.* **254** (2007) 99.
- [179] J. Ghijsen, R.L. Johnson, A. Elschner, N. Koch, *J. Alloys Comp.* **382** (2004) 179.
- [180] J. Ivanco, B. Winter, F.P. Netzer, M.G. Ramsey, L. Gregoratti, M. Kiskinova, *Appl. Phys. Lett.* **85** (2004) 585.
- [181] N. Koch, A.C. Dürr, J. Ghijsen, R.L. Johnson, J.J. Pireaux, J. Schwartz, F. Schreiber, H. Dosch, A. Kahn, *Thin Solid Films* **441** (2003) 145.
- [182] G. Kaune, M.A. Ruderer, E. Metwalli, W. Wang, S. Couet, K. Schlage, R. Rohlsberger, S.V. Roth, P. Müller-Buschbaum, *ACS Appl. Mater. Interf.* **1** (2009) 353.
- [183] M.B. Huang, K. McDonald, J.C. Keay, Y.Q. Wang, S.J. Rosenthal, R.A. Weller, L.C. Feldman, *Appl. Phys. Lett.* **73** (1998) 2914.
- [184] A.C. Dürr, F. Schreiber, M. Kelsch, H.D. Carstanjen, H. Dosch, O.H. Seeck, *J. Appl. Phys.* **93** (2003) 5201.
- [185] L. Lozzi, S. Santucci, S.L. Rosa, *J. Vac. Sci. Technol. A* **22** (2004) 1477.
- [186] J. Ivanco, T. Toader, A. Firsov, M. Brzhezinskaya, M. Sperling, W. Braun, D.R.T. Zahn, *Phys. Rev. B* **81** (2010) 115325.
- [187] S.T. Lee, G. Apai, M.G. Mason, R. Benbow, Z. Hurych, *Phys. Rev. B* **23** (1981) 505.
- [188] S.B. DiCenzo, S.D. Berry, E.H. Hartford, *Phys. Rev. B* **38** (1988) 8465.
- [189] M.G. Mason, *Phys. Rev. B* **27** (1983) 748.
- [190] G.K. Wertheim, S.B. DiCenzo, S.E. Youngquist, *Phys. Rev. Lett.* **51** (1983) 2310.

- [191] G.K. Wertheim, S.B. DiCenzo, D.N.E. Buchanan, *Phys. Rev. B* **33** (1986) 5384.
- [192] C. Bittencourt, A. Felten, B. Douhard, J. Ghijsen, R.L. Johnson, W. Drube, J.J. Pireaux, *Chem. Phys.* **328** (2006) 385.
- [193] Q. Fu, T. Wagner, *Surf. Sci. Rep.* **62** (2007) 431.
- [194] J.N. Israelachvili, *Intermolecular and Surface Forces*, Academic Press, London, 2011.